Diamagnetic Orientation of Inorganic Materials and Its Application to Astrophysics

Hiroki CHIHARA

Thesis Submitted to
Graduate School of Science
Osaka University
for the Degree of
Doctor of Science (Physics)

1999

Abstract

It is known that the non-magnetic micro-crystals dispersed in liquid may align in the magnetic field due to the intrinsic diamagnetic anisotropy of the crystals. This phenomena is referred to as the diamagnetic orientation. The present thesis reports the results of the experiment of the diamagnetic orientation for several inorganic materials. The mechanism of the diamagnetic orientation is considered with three parameters namely the temperature, the grain size and the intrinsic anisotropy of the material. The field H_S required for full orientation, based on the theory of Boltzmann distribution, is expressed by $H_S = \sqrt{15k_BT/N\Delta\chi}$, where T, N, $\Delta\chi$ and k_B are the temperature, the number of mulecules per a grain, the intrinsic diamagnetic anisotropy of the material and Boltzmann constant, respectively.

In the low viscous medium the experimental results of H_S-dependence on these three parameters were consistent with the relation above. In the low temperature region approximated to solidifing point of the medium, the observed H_S-values largely deviate from the theoretical value. In the high viscous medium at room temperature, the observed H_S-values show a substantial excess from the theoretical value. For graphite particles with 2.6μm in average diameter, the observed H_S-value at viscosity $\eta = 11500$cp is about four times larger than the value at $\eta = 2$cp. These results suggest that the H_S-value strongly depends on the viscosity of the medium besides the three parameters.

The origin of this deviation can be explained from the effect of the particle size distribution. It is assumed that the large particles are suffered from the effect of the viscosity resistance, and the motion of the large particles is restricted in the high viscous medium. Consequently the value of H_S increases since the only small particles can orient in the high viscous medium.

This effect of the size distribution appears in low viscous medium as the deviation of

the observed curves with respect to the theoretical $\langle m \rangle$-H curves, where $\langle m \rangle$ and H is the degree of orientation and the magnetic-field strength. The degree of the deviation is estimated with the value of quality of fitting (QF). The values of QF turned out to be $8.14 \times 10^{-4} \pm 4.0 \times 10^{-4}$ and $1.85 \times 10^{-2} \pm 1.2 \times 10^{-2}$ for the sample ensembles of which the half-width of the distribution are 0.22 and 0.60, respectively.

The possibility of the diamagnetic orientation to the interstellar environment is discussed based on the experimental results. As the dependence of the diamagnetic orientation on temperature and grain size is considered, an applicable region for the diamagnetic orientation is the dense region such as molecular cloud core and proto planetary disk. This is because the temperature of the grain is low and the grain size is large in the region due to the effect of the gas-grain collisions. The higher magnetic field is expected in the circumstellar of the young stellar object, if the star formation process is progressing in such a region. The diamagnetic orientation is a possible candidate of the mechanism of grain alignment in the dense region.

Contents

Chapter 1

Introduction

In the early days with respect to modern magnetism, P.Curie classified materials into three groups by their magnetic properties namely ferro-, para- and dia-magnetic states. The first and second groups possess spin moments as the carrier of their magnetic properties. While the third group, referred to as the diamagnetic material, contains no effective spin moments.

A small magnetic moment is produced in the diamagnetic material, in the opposite direction to external magnetic field. This moment is explained in terms of the diamagnetic currents of the localized electrons. Although diamagnetism is a general property seen in all molecules, ions and atoms, their susceptibility are three to four orders of magnitudes smaller than that of the spin moments. Therefore, almost all the studies of the magnetic materials are concerned with the electron spins of the magnetic elements.

The study of magnetic anisotropy was carried out systematically for the first time by Krishnann and Banerjee (1933). They measured the magnetic anisotropy for both magnetic and non-magnetic materials using a newly developed method. The aromatic molecular crystals have prominently large anisotropies among the non-magnetic materials. Pauling (1936) explained the origin of the diamagnetic anisotropy observed in the aromatic molecules in terms of the spatial anisotropies of the molecular bonding orbitals. The study of this mechanism was extended to other organic molecules which consist of various types

of bonding orbitals (Pauling 1979). The discussions led to the experiment of the magnetic orientation due to the diamagnetic anisotropy on organic materials of various sizes, from single aromatic molecules (Cotton and Mouton 1907; Yamagishi et al. 1984) to micron-sized biological systems such as blood cell, fibrinogen (Yamagishi et al. 1989), DNA fiber and biological membrane (Maret et al. 1985). More recently the magnetic effect on crystal growth has been studied for organic crystal of lysozyme and ferritn for example (Sazaki et al. 1997). By use of an optical birefringence, namely the Cotton-Mouton effect (Cotton and Mouton 1907), the detection of the diamagnetic orientation of single molecules was measured with high sensitivity. The theory to explain the magneto-orientation process of small particles observed by the Cotton-Moutton effect was first developed by Langevin (1910) and Born (1918), and extended later on by Beams (1932), Buckingham et al. (1956), Peterlin et al.(1939), Twersky (1969) and Yamagishi et al. (1989).

In the case of single molecule, the degree of orientation remained in the order of 10^{-6} at maximum field of 40 tesla, since the anisotropic energy was much smaller compared with the thermal energy $k_{\mathrm{B}}T$. The full orientation was achieved below several tesla for most of the micron-sized materials. The temperature dependence on the Cotton-Mouton effect was measured in the pulsed high-field up to 40 tesla by Yamagishi, Nagao and Date (1984), and the results were explained by introducing an additional term representing the intermolecular correlations. Consequently the Curie-Weiss constant appeared in the high-field diamagnetic susceptibility of chlorobenzene and nitrobenzene.

The orientation and its related effects of the bio-molecules in a magnetic field have been reviewed in details by Maret and Dransfeld (1985), and various types of magnetic orientations of bio-organic materials have been reported on various polymers, liquid crystals and biological membranes. The degree of orientation has been analyzed basically in terms of thermal equilibrium. Motions due to diamagnetic effects of bio-molecules are reported on macro-molecules, proteins and red blood cells. For example, the magnetic orientation

of long DNA chains or other polymers was investigated and it was revealed that the chains can be oriented about 1% in the field of 20 tesla for DNA chains. In the case of red blood cell with radius $\simeq 8\mu$m, the orientation is completed below 4 tesla (Yamagishi et al. 1984; Mizuno 1994).

The polymerization of fibrinogen was observed in the static field of 8 tesla. The diamagnetic anisotropy of the micron-sized bio-systems is obtained from the relation between the degree of orientation and the field strength. The values of published data of various systems were compiled by Yamagishi (1990). Biological membranes show a strong orientation in a magnetic field due to their intrinsic anisotropic structure, and the degree of orientation depends on the phase transition of the membrane (Maret et al. 1977).

In addition, diamagnetic molecules are expelled or attracted into the region of the maximum magnetic field in a field with strong gradients. These phenomena are effective to separate the macromolecules from the rest of the solution (Simonsen et al. 1974; Melville et al. 1975; Owen 1978). Consequently, the demagnetic effect also causes a rotation of diamagnetic particles, when the geometrically anisotropic particle is placed in an area of significant field inhomogeneity with the scale comparable to the particle. Therefore the geometry of the field inhomogeneity as well as that of the particle should be evaluated prior to the experiment of diamagnetic grain orientation.

These full orientations of micron-sized material occur because the total diamagnetic anisotropy energy of the material becomes considerably large compared with the thermal energy which randomizes the direction of the particle in the high field. In the micron-sized materials, the principle axis of the anisotropy ($\Delta\chi$) of individual organic molecules is aligned along a certain axis of the micron-sized body. Therefore, the magnetic orientation is realized even under relatively low magnetic field, since the total anisotropy of the body is compiled to $N\Delta\chi$. Here, N denotes the number of molecule in the body.

As for the inorganic materials, the diamagnetic anisotropy was observed by Krishnann

and Banerjee (1933) for some basic non-magnetic materials such as quartz, witherite and calcite. However these results did not extend to the discussion on the origin of their anisotropy, since the values were very small compared to that of the organic materials. Moreover, it was necessary to prepare a single crystal of high quality, which was free of magnetic ions, in order to perform the precise measurements on the diamagnetic anisotropy. This condition was difficult to realize most of the oxide crystals.

The diamagnetic anisotropy of inorganic materials is usually much smaller than that of paramagnetic ions, and its possibility to various magnetic applications has been ignored under laboratory environments. The phenomena of magnetic orientation in natural conditions have been analyzed only in terms of the electron-spin moment so far, since the diamagnetic anisotropy had been ignored for the inorganic materials composing the natural solid phase. Recently, the field-induced harmonic oscillation was observed for cm-sized single crystals of quartz, corundum and calcite (Uyeda et al. 1993). Through the observations, a method has been established to compile the diamagnetic-anisotropy data for various inorganic materials. It has become clear that diamagnetic oxides generally posses the efficiency of magnetic orientation. It was expected that micron-sized oxide crystals may generally cause orientation at a relatively low field of several tesla.

The present thesis concerns with the systematic study on inorganic micro-crystal alignment. By the measurement on inorganic micro-crystals it has become possible to evaluate the effect of various parameters on the magneto-ordering process, these parameters being temperature, grain size, the intrinsic anisotropy of the material and the viscosity of the suspending medium. The possibility is discussed on the application on the grain alignment in natural conditions, for example in the Galactic plane.

Chapter 2 reviews the origin of the diamagnetic anisotropies which is the cause of magnetic orientation, and also the method to determine the diamagnetic susceptibilities. The significance of the magnetic field in interstellar space and the mechanism of interstellar

grain alignment are reviewed in Chapter 3. The experimental and analytical procedure of diamagnetic orientation performed in the present work are described in Chapter 4, and the results of the experiments are given in Chapter 5. The viscosity dependence of the field strength required to orient the diamagnetic particles is discovered in the course of an experiment in the low temperature region. The results and discussion on the experiment on the viscosity effect are given in Chapter 6. Finally in Chapter 7 the possibility is discussed on the diamagnetic orientation in the interstellar environment. It is noted that the major components of the cosmic solid-phase are diamagnetic materials. Therefore the diamagnetic orientations of inorganic grains may be applied to magnetic ordering in various fields of science and technology.

Chapter 2

Diamagnetic Anisotropy of Inorganic Materials

2.1 Origin of Diamagnetic Anisotropy

As discussed in the introduction, the origin of the diamagnetic anisotropy ($\Delta\chi$) of individual oxide crystal is an essential factor which determines the intrinsic efficiency of magneto-rotation. This $\Delta\chi$-dependence will be discussed in detail in Chapter 5. The origin of the anisotropies was attributed essentially to the anisotropy of the average of the square radius of the electron-orbit, $\langle r^2 \rangle$. According to the classical Langevin model on diamagnetism, the diamagnetic susceptibility is described as

$$\chi = -\frac{e^2}{6mc^2} \sum_i \langle r_{i^2} \rangle \quad , \tag{2.1}$$

where $\langle r^2 \rangle$, e, m and c is the average radius of the electron-orbit, the electron-charge, the mass of electron and the speed of light, respectively (Langevin 1933). The summation $\sum$ is preformed over all the electrons consisting the molecule. The diamagnetic anisotropy of benzene and other aromatic molecules was explained in terms of the characteristics of the hybridized π-bonding orbital which is spatially extended parallel to the molecular plane.

The diamagnetic anisotropies reported recently in the oxide minerals (Uyeda et al. 1991) cannot be explained in terms of the conventional models mentioned above. Considering the crystal structures of oxides, the [MO_6] octahedral unit and the [MO_4] tetrahedral unit

are the basic components for most of inorganic the oxides crystals. In a cubic structure the units hold the regular symmetry, and the $\Delta\chi$-values between the equivalent principle axis are zero. In a crystal structure with lower symmetry, the octahedral [MO_6] unit is preferentially deformed rather than the tetrahedral unit, the bond direction in the [MO_6] unit being slightly tilted toward the (001) plane. The angle between the bond direction and (001) plane is $\Psi = 35.7°$ when the [MO_6] unit holds the regular symmetry. The angle reduces to $\Psi = 34.5°$ for corundum, $\Psi = 32.1°$ for kaolinite, and $\Psi = 31.5°$ for talc and muscovite. The value of $\Delta\chi$ tends to increase with the reduction of Ψ. Moreover the oxides all have an easy-plane type of anisotropy, in which the principal axes lie in an arbitrary direction in the (001) plane.

For oxides composed of light elements, the diamagnetic susceptibility is caused mainly by the bonding-orbital electrons of the O^{2-} ions, according to the Pascal rule (e.g. Gupta 1983). The spatial distribution of the bonding-orbital electrons of individual M-O bond is generally anisotropic, the principal axis of anisotropy pointing in the M-O bond direction. Hence one may assume an anisotropy in the diamagnetic susceptibility that emerges from the individual bonding-orbital electrons.

The field-induced anisotropic energy for an M-O bond, which has the direction cosine (α, β, γ), is calculated by the following equation:

$$U(H) = -\frac{1}{2}H^2\{\chi_{bd\perp} + \Delta\chi_{bd}\left(a^2\alpha^2 + b^2\beta^2 + c^2\gamma^2\right)\} \quad , \tag{2.2}$$

where $\chi_{bd||}$ and $\chi_{bd\perp}$ denote the susceptibilities parallel and perpendicular to a bond directions, respectively (Uyeda 1993). The anisotropy is defined as $\Delta\chi_{bd} = \chi_{bd||} - \chi_{bd\perp}$. The direction cosines of magnetic field, H, are denoted as (a,b,c). The x-, y- and z-coordinates are taken along the a-, b- and c*-axes of the crystal, respectively. The c*-axis is denoted as the axis perpendicular to the (001) plane. The χ tensor for per molecular formula of the individual oxide is calculated from the sum of the tensor components of each M-O bond

derived from equation(2.2), which essentially follows the summation method by the Pascal rule. The susceptibility of an [MO_6] octahedral unit, χ_{octa}, in the magnetic field, $H(a,b,c)$, is described as

$$\chi_{octa} = 4\chi_{bd\perp} + 2\chi_{bd\parallel} + \Delta\chi_{bd}\left(a^2\sum\alpha^2 + b^2\sum\beta^2 + c^2\sum\gamma^2 - 2\right) \quad , \tag{2.3}$$

where $\sum\alpha^2$, $\sum\beta^2$ and $\sum\gamma^2$ denote the sum of the direction cosines of the six M-O bonds composing the octahedral unit. When the unit holds the regular octahedral symmetry, as is the case of cubic crystals, χ_{octa} is equivalent between the principal axes to

$$\chi_{octa} = 4\chi_{bd\perp} + 2\chi_{bd\parallel} \quad . \tag{2.4}$$

The sum of the anisotropies of the six bonds will cancel out and hence will not affect the total susceptibility explicitly. The susceptibility of an O^{2-} ion can be treated as an isotropic diamagnetic component, as it has been done in the case of the conventional Pascal rule. The anisotropic susceptibility of the [MO_6] unit, $\Delta\chi_{octa}$, becomes zero. When the symmetry is distorted and Ψ deviates from $\Psi = 35.7°$, the sum of the anisotropy for the six bonds will not cancel out. The intrinsic anisotropy emerges in the octahedral unit. In general $\Delta\chi_{octa}$ is calculated from equation(2.3) as

$$\Delta\chi_{octa} = \Delta\chi_{bd}\{\left(\sum\alpha^2\right) - \left(\sum\alpha^2 - \sum\beta^2\right)b^2 - \left(\sum\alpha^2 - \sum\gamma^2\right)c^2\} \quad . \tag{2.5}$$

The two-axial type anisotropy is expected when the condition $\sum\alpha^2 > \sum\beta^2 > \sum\gamma^2$ is realized, with x-, y- and z- are the easy, second easy- and the hard-axes, respectively. This type of anisotropy is expected for orthorhombic symmetry. When the direction cosines have the relation, $\sum\alpha^2 = \sum\beta^2 > \sum\gamma^2$, the crystal has easy-plane anisotropy, in which the principal axis has an arbitrary direction in the ab-plane.

The quantity $\Delta\chi_{ocat}$ is calculated as

$$\Delta\chi_{octa} = -\Delta\chi_{bd}\left(\sum\alpha^2 - \sum\gamma^2\right)c^2 \quad . \tag{2.6}$$

This type of anisotropy is expected for corundum as well as for the sheet silicates. The uniaxial-type anisotropy may occur when $\sum\alpha^2 = \sum\beta^2 < \sum\gamma^2$.

The diamagnetic anisotropy par molecular formula, $\Delta\chi_{cal}$, of a given oxide crystal may be calculated empirically when the numerical values of $\sum\alpha^2$, $\sum\beta^2$ and $\sum\gamma^2$ are known in equation(2.5). These values are easily obtained from the atomic position data of each crystal.

The relation between $\Delta\chi_{cal}$ and the measured $\Delta\chi$-values per molecular formula showed that the major origin of the diamagnetic anisotropy of the oxides is strongly related to the spatial anisotropy of the individual chemical bonds of the octahedral [MO_6] unit. Consequently it was revealed that diamagnetic oxides, with the exception of cubic crystals, generally posses the efficiency of magnetic rotation at a finite field intensity. The efficiency of diamagnetic orientation of a micro-crystal oxide-grain depends strongly on its crystal structure. It is expected that the values of H_S (the field of full orientation) may vary nearly two orders of magnitude among different sheet-silicate grains of the same size and temperature.

2.2 Measurement of Diamagnetic Anisotropy

As mentioned before, most of the $\Delta\chi$-values of inorganic materials are very small compared to those of organic materials or those caused by the magnetic ions, which cannot be obtained by the conventional methods for the anisotropy measurements. In the measurements on magnetic anisotropies performed by Krishnann and Banerjee (1933), mentioned in the introduction, the $\Delta\chi$-values were determined from the observations of the field-induced harmonic oscillation of the sample. The anisotropies of ice (Lonsdale 1949) as well as corundum (Rao and Leeha 1953) were measured by the so-called "*Klishnann's critical torsion method*". Most of the contemporary methods of measuring magnetic anisotropy are based on Klishnann's method. However the detection limit of these methods is on the

order of about 10^{-9}emu/cc, and it is difficult to detect the small diamagnetic anisotropies of various oxide crystals at this sensitivity.

A method using the harmonic oscillation was developed in the static field up to 1.7T (Uyeda 1993a, b) for the purpose of measuring the $\Delta\chi$-values of diamagnetic oxides. The method is based on the characteristics of the crystal rotational-motions in the high-field condition. The contribution of the restoring force of the string suspending the sample would become negligible as the field-induced energy increases. This is realized by increasing the size of the single crystal, by increasing the field intensity or else by minimizing the restoring force of the string. In this condition, the period of harmonic oscillation induced by the magnetic anisotropy becomes proportional to the reciprocal of the field, with no contribution of the restoring force of the string.

In this method the cm-sized single crystals were used to improve the sensitivity. The crystals were shaped into a cylindrical rod, the diamagnetic hard- and easy-axes being located in the basal plane of the rod. In many cases the c-axis corresponds to the hard-axis for the diamagnetic oxide crystals. The small rotation of the crystal was detected by the variation of the laser-beam intensity transmitted through the crystal. The relation between field intensity, H, and the period of rotational harmonic oscillation, τ, was observed and analyzed as follows. Provided that the amplitude of the rotational angle is small enough, the equation for the rotating crystal rod is described as $I\,\frac{d^2\theta}{dt^2} = -H^2N\Delta\chi\theta - \left(\frac{D}{\ell}\right)\theta$, where I and N denote the moment of moment of inertia and the mole number of the sample, respectively. The tensional rigidity and the length of the string are denoted as D and ℓ, respectively. The symbol θ denotes the angle between the easy axis and the direction of the field.

In a high-field region, where the second term becomes negligible compared to the term of field-induced anisotropic energy, the period of oscillation, τ, is described as $\tau = 2\pi\left(\frac{I}{N\Delta\chi}\right)^{1/2} H^{-1}$. The period becomes proportional to the field intensity with no

effect of the parameters of the restoring force, D and ℓ. The magnetic anisotropy of the sample is calculated numerically using the above equation of motion and τ.

The sensitivity of the method was estimated to be (1.2×10^{-12}emu/cc, provided that a mole-sized single crystal of the above mentioned geometry is available (Uyeda, Chihara and Okita 1998). The high sensitivity has been achieved because the large-sized crystal was obtainable due to the recent progress on synthetic crystal growth, and also because the fluorocarbon string with small tensional rigidity was introduced in the experiment. In the conventional method the tensional rigidity of the fiber suspending the sample was comparable to the field-induced energy of the sample. This condition causes the limitation to the sensitivity of the anisotropy measurements.

As it will be described in Chapter 4, the $\Delta\chi$-values of the material are obtained from the analysis of the dependence of degree of orientation on the magnetic field. It is seen, however, that the amount of uncertainty was considerably large due to the deviation of N-value of the suspended micro-crystals. It is noted that the $\Delta\chi$-values should be determined independently from precise anisotropy measurements in order to investigate the quantitative the effects of various parameters, such as temperature and viscosity of the suspending medium, on the grain-orientation process. It is described in Chapter 5 that the method of micro-crystal orientation is the only method to estimate the diamagnetic anisotropy for the minerals with difficulty of obtaining the single crystal.

Chapter 3

Interstellar Magnetic Field

3.1 Detection of Interstellar Magnetic Field

It is concluded from the observation along the Galactic plane that a weak magnetic field of the order of several micro-gauss is omnipresent in the Galaxy. The magnetic field is considered to play an important role in various celestial hierarchies and as well as in various physical processes. Although the importance of the interstellar magnetic field has been discussed to a large extent theoretically (e.g. Zweibel 1987), only a few reports on magnetic field based on direct observations have been made, partly because of the difficulty of the direct detection of the faint magnetic field, which is less than 100μG.

The interstellar magnetic-field vector $\boldsymbol{B}$ is divided into two components, which are parallel and perpendicular to the line of sight [1] denoted as $B_{||}$ and $B_{\perp}$, respectively. At this time, there are no methods which are able to measure both components simultaneously. The standard methods to carry out magnetic field observations are as follows (Heiles 1987):

1. Polarization of synchrotron radiation ($B_{\perp}$)

2. Faraday rotation of the radiation from the polarized sources due to interstellar medium ($B_{||}$)

3. Zeeman effects of interstellar molecules ($B_{||}$)

[1] line of sight : the line between the object and the observer.

4. Visible and infrared interstellar polarization of star lights due to the alignment of interstellar grains ($B_\perp$)

The synchrotron radiation is caused by the Lorenz motions of free electrons in the diffuse area, where the electron velocity may approach light speed. This polarization becomes either circular or liner depending on the angle between the direction of the magnetic field and the line of sight. In this method, the observer is able to obtain the information about the direction of the magnetic field. The intensity of the magnetic field will be inferred indirectly from the radiation intensity. It is seen that the method cannot be used to estimate the field of the dense regions such as the molecular clouds of the star formation region. The method is effective to detect the magnetic structure of a wide spatial area such as whole outer-galaxy. Figure 3.1 shows the example of the measurements in terms of this method for the field structure of the outer spiral galaxy M51. The observed field direction generally points along the spiral arms in a galaxy.

The Faraday rotation is observed on the polarized radiation sources such as the synchrotron radiation or the pulsars. The rotation occurs while the radiation propagates through the interstellar medium. The rotation angle of the plane of polarization ψ is given by

$$\psi = RM\lambda^2 \quad [\text{rad}] \tag{3.1}$$

$$RM = 8.12 \times 10^5 n_e B_{||} L \quad [\text{rad/m}^2] \tag{3.2}$$

where ψ is the polarization angle, λ [m] is the wavelength of a radiation source, RM is a physical variant referred to as the rotation measure, $B_{||}$ [Gauss] is the field component in the direction of propagation, L [m] is the distance of the propagation in the interstellar matter and n_e [cm^{-3}] is the number density of free electrons. From equation(3.1), the radiation from a polarized source with an initial angle ψ_0 is observed as $\psi = \psi_0 + RM\lambda^2$. The value of RM and the initial polarization angle ψ_0 will be obtained from the values of ψ

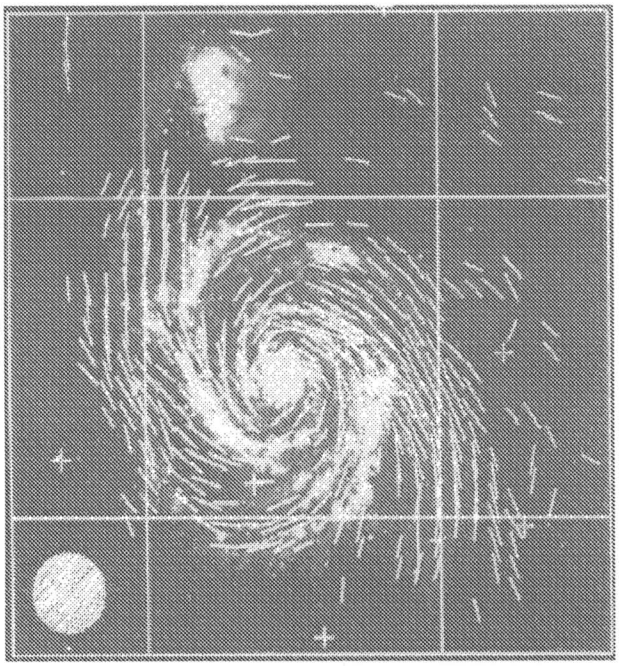

Figure 3.1: The large scale magnetic field of M51 as revealed by radio continuum polarimetry. (Neininger 1992)

observed at various wavelengths. By inserting the values n_e and L, which are inferred from other observations, the average $B_{||}$-value is obtained for the interstellar matter between radiation source and the observer. According to the observation of pulsars, the average galactic magnetic field was obtained for the area within a radius of approximately 10^4 light-years from the solar system. The estimated field intensity was several micro-gauss with the direction along to the Orion-Cygnus arm, which is one of the major spiral arms of our Galaxy. The results are consistent with the synchrotron observation on the whole spiral galaxy seen in Figure 3.1.

The method using the Zeeman effect is one of the most classical methods to measure the magnetic field in astrophysics. Although this method is useful for high-field detection such as the sunspot, it is difficult to measure the faint field such as interstellar magnetic field, mainly because of the Doppler shift of the exited lines caused by the local motion

of interstellar medium. Verschuur (1969) detected the Zeeman effect of 21-cm radio wave from the neutral hydrogen region (HI region) for the first time and revealed the magnetic structure of several micro gausses along to the galactic arms. Recently, the magnetic structure of star formation region has been observed with the Zeeman effect for the OH molecular clouds in constellation Ophiuchus and Taurus (Troland et al 1996).

The interstellar linear polarization of star light is considered to occur by the preferential extinction due to geometrically anisotropic-dust particles in the line of sight, since the degree of polarization and the degree of extinction due to the grains are well correlated for the observed star lights. Since the interstellar polarization indicates the maximum degree at $4000 - 6000$ Å in the visible wavelength, the shape and the size of the grain are inferred to be elongated ellipsoid of approximately 0.1μm.

The origin of this polarization is considered as follows (Figure 3.2). When the light from the star propagates through the cloud of grains, the incident light which has the vibration plane parallel to the longest axis of the grain is suffered from the larger absorption and scattering than that of perpendicular component. Consequently, we observe the polarized light of which the vibration plane is perpendicular to the longest axis of grains, provided that the longest axes of grains along to the line of sight are preferentially aligned in a certain direction. Figure 3.3 shows the polarization map along the galactic coordinate (Axon and Ellis 1976). The length and the direction of solid lines in this figure indicate the degree and the direction of the polarization, respectively. As a whole, the polarization planes are aligned parallel to the Galactic plane indicating that the grains are alignment perpendicular to the Galactic plane. It is generally considered that the grain alignment is caused by the Galactic field, since the polarization pattern of Figure 3.3 coincides with the field distribution obtained by the methods 1 to 3. If we accept the assumption that some interaction exists between the grains and magnetic field which makes the grains orient, the field direction can be obtained for the component perpendicular to the line of

sight. However, one cannot determine the strength of the magnetic field directly due to the quantitative uncertainty of the relation between the magnetic field and the grain alignment.

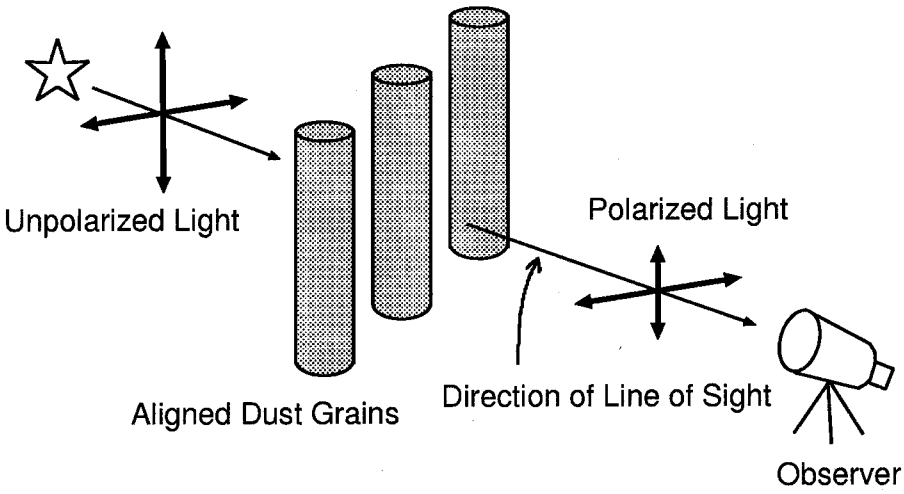

Figure 3.2: The mechanism of polarization caused by the elongated grains.

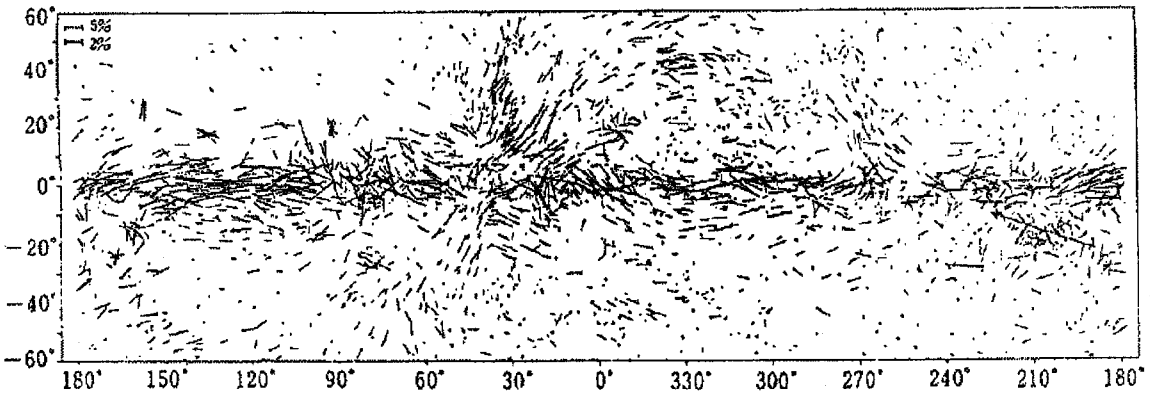

Figure 3.3: The polarization map on galactic coordinate. (Axon and Ellis 1976)

3.2 Mechanism for Interstellar Grain Alignment

The observations which have been carried out are restricted to obtain the information of the magnetic structure especially of the star formation region. Among them, the observation in terms of the method 4 is carried out extensively. This is because this method requires a polarimetric observation of individual star light, which is a considerably simple procedure compared to the methods 1 to 3. The spatial resolution of the method 4 is the highest among the four methods. It is noted that the methods 1 to 3 are based on well established electro-magnetic principles. The obtained intensity and direction of the field are consistent with each other. Whereas the method 4 is based on the fact that its result assumed is consistent with the results of other methods; that is, the pattern of polarization seen in Figure 3.3 coincides with the field distribution estimated by the Zeeman effect or the Faraday rotation. The mechanism to explain the grain alignment which should serve as a theoretical basis of the method, is based on assumptions that may be effective only in interstellar environment.

The conventional theory of the grain alignment was first presented by Davis and Greenstein (1951). According to this theory (hereafter referred to as the DG theory), the paramagnetic relaxation occurs on the grain. This happens because the electron spins of the minor magnetic ions suffer rotational magnetic field caused by the thermal rotation of the grains. Due to the collisions between the grains and the gas particles, the rotation about the axis with the largest moment of inertia is preserved considering a long time period. In the DG theory, the rotational kinetic energy of the grain is equivalent to the thermal energy of the gas particles. In generall, the magnetic susceptibility of the object in the rotating magnetic field is described as $\chi = \chi' + i\chi''$. The rotation about the axis perpendicular to the magnetic field is gradually dumped in order to diminish the imaginary part of susceptibility, χ'', and the rotation about the axis parallel to the field will be preserved.

Approximately after 10^7 years, the rotation axis of the grains is aligned along the direction perpendicular to the magnetic field. Here the time-scale of orientation due to the DG theory (t_r) and of disorientation due to the gas-grain collisional effect (t_c) are compared. It is noted that $\delta = t_c/t_r \geq 1$ should be satisfied to preserve the alignment. The theoretical details on this subject are reviewed by Spitzer (1978) and Greenberg (1978).

The degree of orientation of the actual interstellar grain estimated from the polarimetric observation turned out to be exceedingly larger than it was expected from the DG theory. The low concentration of electron-spins as well as the faint interstellar field could not account for the observed degree of polarization quantitatively. In order to improve the model, the existence of the superparamagnetic phase was assumed in the interstellar grain (Spitzer 1987). Hence the imaginary part of the susceptibility, χ'' may increase by a factor of 10^5 compared to the value given by the DG theory, and the value of t_r can be short enough to achieve $t_c/t_r > 1$. Another improvement was made by assuming that the angular velocity of the grains exceeds the corresponding thermal energy of the gas particles by the factor of 10^4 or more (e.g. Purcell 1977; Spitzer and McGlynn 1979; Lazarian 1995). These assumptions are now widely accepted for the discussion of grain alignment in the diffuse interstellar region from the qualitative point of view.

Furthermore the DG theory is applied to the dense interstellar region when the magnetic field is considered to play an important role on star formation process. This problem will be discussed in detail in Chapter 7.

Chapter 4

Experimental

4.1 Experimental Procedure

4.1.1 Sample Preparation

Suspensions of the sample grains were prepared, and the grain sizes were classified by the precipitation method. After settling the suspension for several weeks, the classified size distribution samples can be obtained in the different layers of the suspension. The size distribution was determined by SEM (scanning electron microscopy) images, to estimate the average mole number of a particle. The typical example of the SEM image of the graphite sample is shown in Figure 4.1. Various parameters of the prepared samples are shown in Table 4.1.

4.1.2 Experimental Setup

Setup at room temperature

Figure 4.2 shows an example of the experimental setup to measure the diamagnetic microcrystal orientation at room temperature. After settling the sample suspension maintained in a quartz cell at the center of the experimental space, a He-Ne laser beam was transmitted through the suspension in a direction perpendicular or parallel to the field. Due to the optical anisotropy of the platy grains, the degree of orientation is monitored quantitatively as a variation of the optical transmitted laser beam intensity with respect

Table 4.1: The physical properties of the samples.

No.	Material	Morphology	Viscosity (cp)	Radius (μm)	Suspension Medium
A1	graphite	disk	$1 \sim 100$	2.5 ± 0.2	ethanol
A2	graphite	disk	$1 \sim 100$	3.8 ± 0.2	-
B1-11	graphite	disk	1.87~11250	2.6 ± 0.13	ethanol & glycerin
C1	graphite	disk	1~700	29.2 ± 29.0	ethanol & glycerin
C2	graphite	disk	1~700	0.38 ± 0.2	-
C3	phthalocyanine	needle?	1~700	3.83 ± 2.3	-
D	kaolinite	disk	~1	$0.6 \sim 1.8 \pm 0.3$	water
E	phlogopite	disk	~1	$0.6 \sim 1.1 \pm 0.2$	water
F	lepidolite	disk	~1	2.0 ± 0.8	water
G	talc	disk	~1	$0.6 \sim 2.4 \pm 0.6$	water

to the random orientation. The direction of the diamagnetic easy axis of the micro-crystal is usually in the c-plane (e.g. Yamagishi et al. 1989). The amount of incident light intercepted by the grain becomes the largest when the c-plane is perpendicular to the direction of the light path. Details of analyzing the optical data are described in §4.2.1.

Setup for examining temperature dependence

The sample cell for examining the temperature dependence of H_S is shown in Figure 4.3. The sample suspension was put inside two-fold dewars: the outer dewar was filled with liquid N_2, and the inner one was filled with ethanol ($\simeq 50\text{cm}^3$), so as to keep the homogeneity of the sample temperature. A heater attached to the sample cell was used to control the temperature. Monitoring of the sample suspension temperature was used with a pair of chromell-alumel thermocouples. This experiment was carried out in the temperature range from 160K to room temperature ($\simeq$ 285K). The direction of the laser beam was parallel to the direction of the field. The path length of the laser beam in the sample suspension is 10mm.

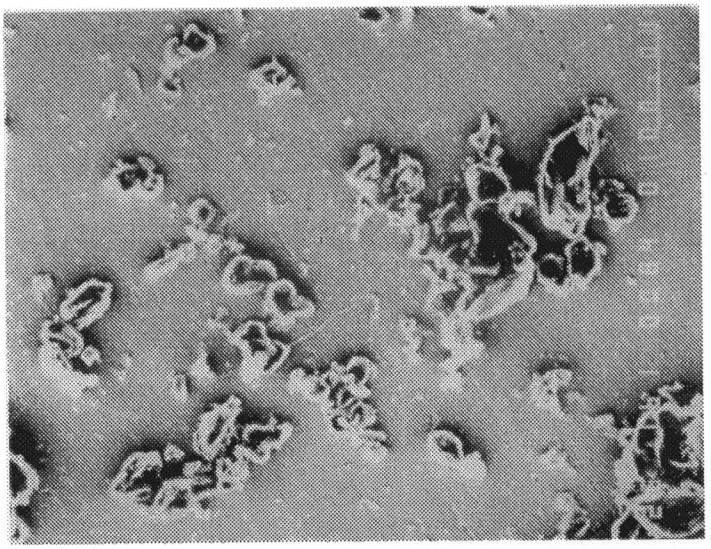

Figure 4.1: The typical example of the SEM image of graphite grain.

Setup for examining viscosity dependence at constant temperature

In order to examine the effect on magnetic orientation, the suspensions were prepared from ethanol and glycerin mixture. The viscosity range of the suspension is from 1.87cp through 11250cp and the variety of the viscosities is realized by the controlling the ratio of the mixture. The measurements for the viscosity of the suspension mediums are carried out with a viscosity meter at the freezing point of water (0°C), and the values of viscosity are measured within 5% in accuracy.

For the purpose of equalizing the grain sizes and measuring the average sizes of the grain, the precipitation method and image processing using the SEM images mentioned in the previous section were carried out. The sample labeled B1-11 in Table 4.1 is used in this setup. The average radius of the sample particles was $2.59 \pm 0.13\mu$m. The thickness of the particles was estimated to be $0.27 \pm 0.06\mu$m. Consequently the difference of the average sizes of the particles between different samples was less than 20%.

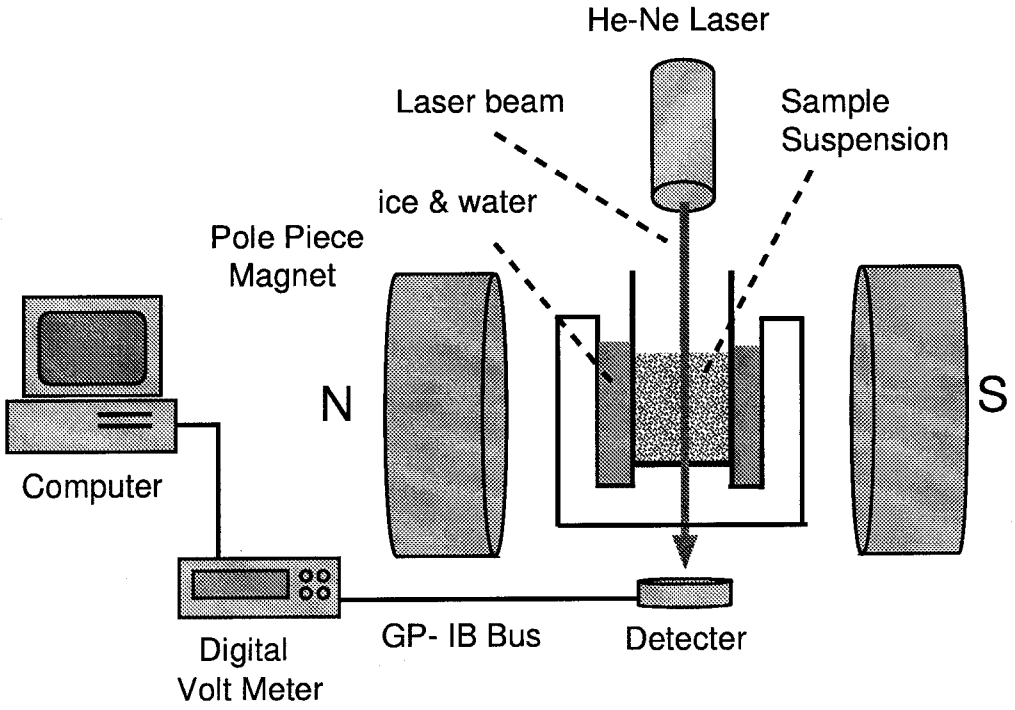

Figure 4.2: Experimental setup for diamagnetic orientation. The variation of intensity of the transmitted beam through the sample suspension is detected with a photo diode.

4.2 Analytical Procedure

4.2.1 The Analysis of Diamagnetic Orientation

The field-induced energy U is expressed for a molecule with the anisotropic diamagnetic susceptibility, $\chi_{||}$ and $\chi_{\perp}$, which are respectively along the parallel and perpendicular directions to the diamagnetic easy axis of the molecule as

$$U = -\frac{H^2}{2}(\chi_{\perp} + \Delta\chi \cos^2\theta) \ , \tag{4.1}$$

$$\Delta\chi = \chi_{||} - \chi_{\perp} \ . \tag{4.2}$$

where θ is the angle between the magnetic field H and the molecule easy axis. The geometric relation is shown in Figure 4.4.

For the case of micron-sized particles, the field-induced energy is expressed by the equation(4.1) by substituting $\Delta\chi$ with $N\Delta\chi$ due to the alignment of the molecular diamagnetic-

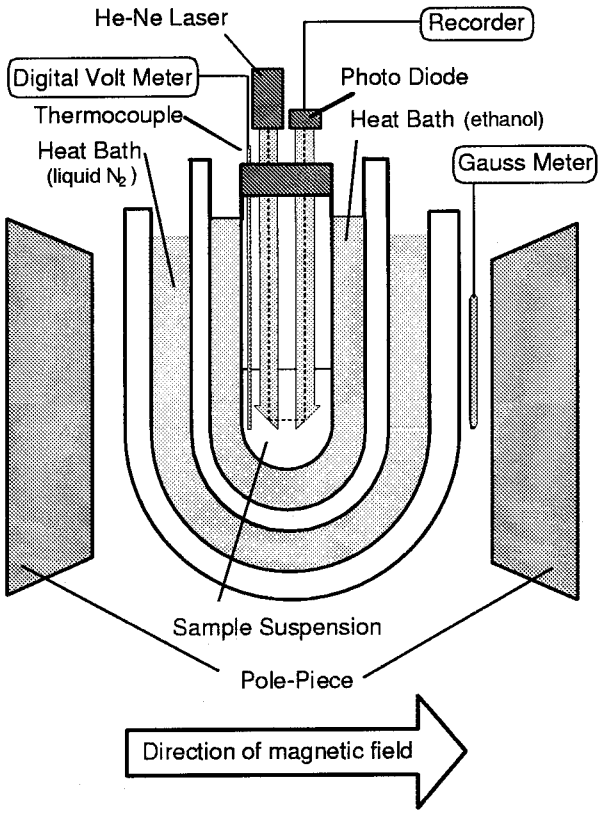

Figure 4.3: Experimental setup for diamagnetic orientation at low temperature.

principle axis in the particle mentioned before, where N is the number of molecules (or chemical formula) included in the grain. The field-induced energy is then described as

$$U = -\frac{NH^2}{2}(\chi_\perp + \Delta\chi \cos^2\theta) \ . \tag{4.3}$$

It is convenient to define an order-parameter $\langle m \rangle$ to describe the degree of grain ordering which is the conventional parameter used to describe the ordering process of liquid crystals. The order-parameter $\langle m \rangle$ is defined as the Boltzmann average of the function, $3\cos^2\theta - 1$, which is calculated as

$$\begin{aligned} \langle m \rangle &= \frac{1}{2}\langle 3\cos^2\theta - 1 \rangle \\ &= \frac{1}{2}\frac{\int_0^\pi (3\cos^2\theta - 1)\exp(-U/k_\mathrm{B}T)\sin\theta d\theta}{\int_0^\pi \exp(-U/k_\mathrm{B}T)\sin\theta d\theta} \ , \end{aligned} \tag{4.4}$$

where k_B is the Boltzmann constant and T is the temperature of the grain and the sus-

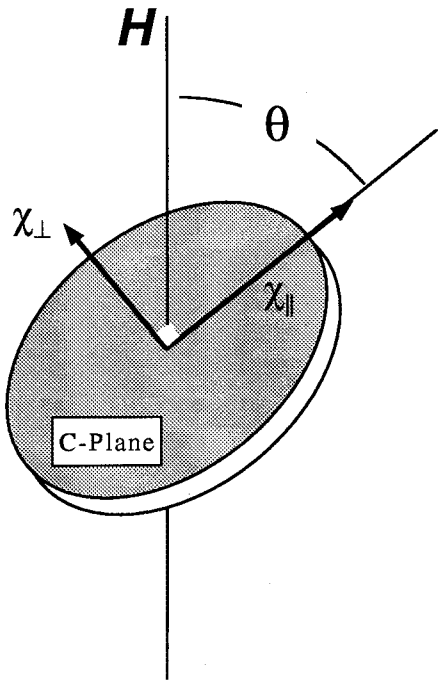

Figure 4.4: Disk grain particle in a magnetic field. C-plane of the grain is parallel to the grain axis. $\chi_{||}$ and $\chi_{\perp}$ are the magnetic susceptibilities parallel and perpendicular to the grain axis, respectively. θ is the angle between the field and the grain axis.

pension medium. The value of $\langle m \rangle$ varies from zero to unity, which corresponds from the completely random state to the completely ordered state.

Equation(4.4) is simply expressed as

$$\langle m \rangle = \frac{3}{4\alpha}\left(\frac{e^{\alpha}}{I} - 1\right) - \frac{1}{2} \quad , \tag{4.5}$$

in which α and I are given as

$$\alpha = \frac{N\Delta\chi H^2}{2k_{\mathrm{B}}T} \quad , \tag{4.6}$$

and

$$I = \int_0^1 \exp(\alpha t^2) dt \quad . \tag{4.7}$$

The relation of equation(4.5) is calculated for various $\Delta\chi$-values as shown in Figure 4.5.

It is seen that the value of $\langle m \rangle$ cannot come to $\langle m \rangle = 1$ at a finite field intensity. Hence the field required to achieve $\langle m \rangle = 0.8$ is defined as the field of full orientation, H_{S},

for the advantage of comparing the measured ordering processes among individual grain-suspensions quantitatively (Uyeda 1991). The H_S-value was derived by extrapolating the linear relation of the zero-field approximation, $\langle m \rangle = 15\alpha/2$, to the point of full orientation $\langle m \rangle = 1$. That is, equation(4.5) can be expanded for the low-field or high-temperature limit ($\alpha \ll 1$) as

$$\langle m \rangle = \frac{2\alpha}{15}\left(1 + \frac{2}{21}\alpha\right) \quad . \tag{4.8}$$

When the field is near zero, the second term of the equation is negligible and a linear relation, $\langle m \rangle = 15\alpha/2$, is seen between $\langle m \rangle$ and α as described by the broken line in Figure 4.6 (Langevin 1910; Yamagishi et al. 1990). Extrapolating the linear relation to the region of $\alpha \gg 1$, the value of $\langle m \rangle$ becomes unity at $\alpha = 15/2$. The actual degree of orientation, $\langle m \rangle$, at this point is obviously below unity $\langle m \rangle = 0.8$, which is calculated exactly by inserting $\alpha = 15/2$ in equation(4.5). In the high field or low temperature limit ($\alpha \gg 1$), it is convenient to calculate $\langle m \rangle$ by the use of the formula obtained by expanding equation(4.5) as

$$\langle m \rangle = 1 - \frac{3}{2\alpha}\left(1 + \frac{1}{2\alpha}\right) \quad . \tag{4.9}$$

Hence, H_S is calculated from the condition $\alpha = N\Delta\chi H^2/2k_BT = 15/2$ as

$$H_S = \sqrt{\frac{15k_BT}{N\Delta\chi}} \quad . \tag{4.10}$$

The solid curve of Figure 4.6 shows the saturation behavior of equation(4.5).

The equation of H_S is understood by considering the balance between the field-induced energy of the grains and the thermal agitation energy from the suspension medium. That is, diamagnetic orientation is achieved when the field-induced energy is at least one order larger than the thermal agitation energy.

4.2.2 Experimental Order Parameter

The experimental value of $\langle m \rangle$ is obtained as the relative intensity of the transmitted light as $\langle m \rangle = \Delta I_i / \Delta I_s$. Here $\Delta I_i = I_i - I_0$ is the variation of light intensity, I_i, in the magnetic field, H_i, with respect to the intensity at no magnetic field I_0. ΔI_s is the saturated value of the variation. This saturation corresponds to the state of the grain ordering, $\langle m \rangle \sim 1$. The calculation was based on the average of light intensity intercepted by the optically anisotropic grains over the various directions of the c-planes. The relation was confirmed experimentally for several diamagnetic materials, where the measured $\Delta I_i / \Delta I_s$-values were compared with the calculated $\langle m \rangle$-H curve of equation(4.4) by use of the published $\Delta\chi$-values and the N-values observed by the SEM images.

The I_0-value after applying the field is confirmed to be identical to the I_0-value before applying the field, with the deviation of less than 1%, in the actual measurement. It is also confirmed that the relation between the applied field and $\Delta I_i / \Delta I_s$-value always follows equation(4.4). Hence the grain directions are considered to be in a completely random state before and after applying the field due to the thermal motions of the suspended-medium molecules. Before performing an individual measurement, the I_0 intensity was monitored to confirm that its transient fractuation is less than several percent with respect to ΔI_s.

4.2.3 $\langle m \rangle$-H Curve Fitting

The $N\Delta\chi$-value and the H_S-value are determined with the least-square fitting of the experimentally obtained $\langle m \rangle$-H plot to the equation(4.4). In order to perform this process, a program was made in a personal computer. For the portability and the ease for cording, Microsoft Visual Basic was selected as the programming language. This program can be run on a personal computer under the Microsoft Windows 3.1 or 95 environment. The screen-shot of the program window is shown in Figure 4.7. In this program two parameters are given as a free parameter for fitting such as $N\Delta\chi$-value and the normalization value. In

practice, equations(4.5), (4.6) and (4.7) are adopted to calculate the theoretical $\langle m \rangle$-value in this program. In equation(4.7), the integral value will be divergent when the index of the exponential function is too large. Therefore the applicable range of the $N\Delta\chi$ is under $\sim 5 \times 10^{-18}$ emu in the case of $H \leq 1$ tesla and $T \simeq 300$ K. The step of the fitting is indicated in the plot window and the least-square value of fitting is indicated in the result window. The part of the source code is in Appendix A.

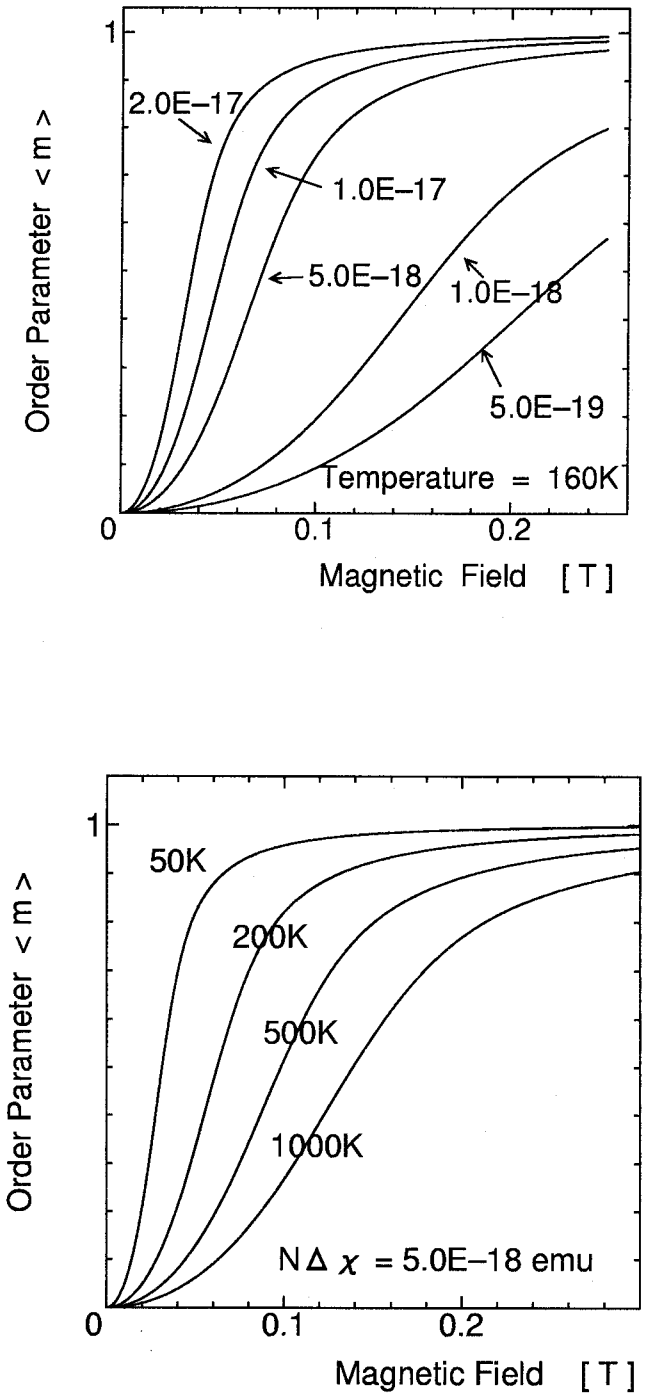

Figure 4.5: Order parameter $\langle m \rangle$ as a function of magnetic field H for various values of $N\Delta\chi$(top) and T (bottom).

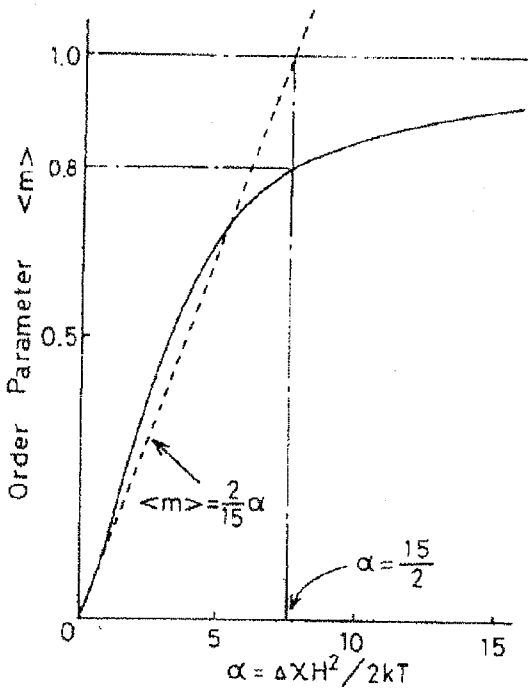

Figure 4.6: Order parameter $\langle m \rangle$ as a function of $\alpha = \Delta\chi H^2/2k_{\mathrm{B}}T$. The full and the dashed lines are given by equation(4.10) and the first term of equation(4.8), respectively. 80% orientation is obtained at $\alpha = 2/15$, which is obtained as the crossing point of $\langle m \rangle = 2\alpha/15$ and $\langle m \rangle = 1$ (Yamagishi et al. 1990).

Figure 4.7: The screen-shot of the windows for $\langle m \rangle$-H curve fitting program on Microsoft Windows platform.

Chapter 5

Results

5.1 H_S Dependence on $\Delta\chi$, N and T

According to the analysis of magnetic grain ordering process based on the Boltzmann distribution mentioned above, it has become clear that the efficiency of magnetic ordering dependents directly on the temperature (T), the intrinsic anisotropy of the material ($\Delta\chi$) as well as the average mole number of the grain (N). In the previous studies on organic materials, it was difficult to examine the relations between the above three parameters in the actual observations. The systematic studies on inorganic materials enable such investigations.

A typical example is shown in Figure 5.1 of the relation between magnetic field H and order-parameter $\langle m \rangle$ for graphite samples labeled A1 and A2. The horizontal axis indicates the field intensity H, while the vertical axis indicates the degree of orientation expressed with the order-parameter $\langle m \rangle$. The solid curves in the figures are theoretical values of $\langle m \rangle$ fitted the measured values with equation(4.4). The experimental values are in accordance with the theoretical values, and it is verified that the orientation is realized with the balance between the diamagnetic anisotropic energy per a grain ($N\Delta\chi H^2/2$) and the thermal energy ($k_B T$).

The relation between the grain size (N) and the field of H_S is shown in Figure 5.2, the broken curves being calculated with equation(4.10). The relations of H_S and N as well as

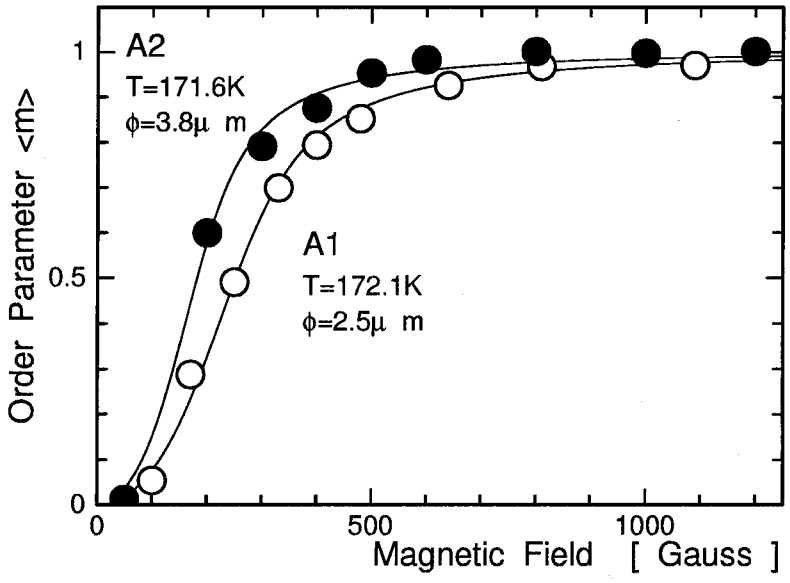

Figure 5.1: Relation between magnetic field, H and the degree of orientation $\langle m \rangle$, for graphite samples A1 and A2 (Chihara et al. 1998).

that of H_S and $\Delta\chi$ are verified as it is expected from the theory of orientation shown by the broken lines.

The relation between H_S and temperature T of suspension is measured on the disk-shaped graphite grains. This experiment was carried out in the temperature range from 160K to room temperature, ethanol being used as a medium for suspending the graphite grains. Figure 5.3 shows the results of the experiment. The curves in this figure are given by the calculation of equation(4.10). The adopted $N\Delta\chi$-value of samples is the mean value of each $N\Delta\chi$-value obtained from each $\langle m \rangle$-H curve in the temperature range from 200K to 260K. This figure shows that the experimental data are in accordance with the theoretical relation, H_S being proportional to $\sqrt{T}$ in the temperature range above 180K.

Most of the measurements on grain-ordering have been focused previously on biological materials, and hence it was difficult to change the condition from biological temperature.

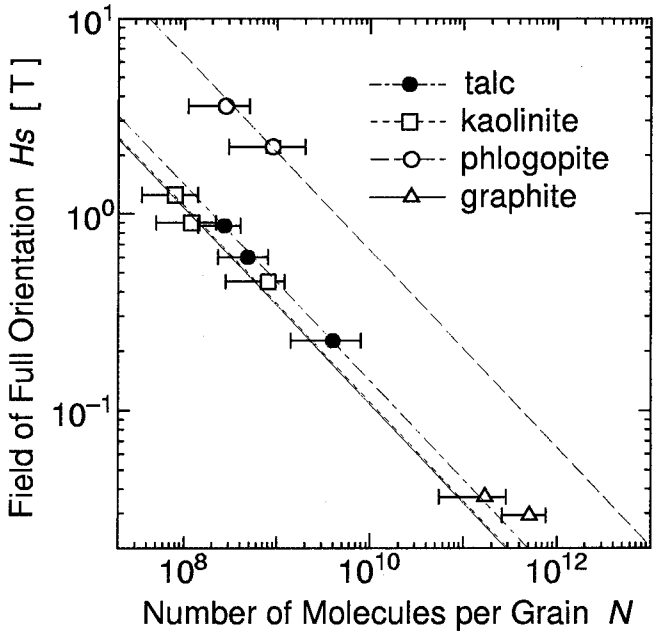

Figure 5.2: Relation between the field of full orientation H_S and number of molecules per grain, N, for the suspensions of talc, kaolinite, phlogopite and graphite. Broken curves are calculated from equation(4.10).

The temperature dependence obtained for inorganic graphite-grains has been examined directly for the first time, and the ordering process is dominated by the thermal energy and the field-induced anisotropic energy.

The average diamagnetic anisotropy per a grain particle in each sample is $N\Delta\chi = -3.6 \times 10^{-17}$emu and $N\Delta\chi = -5.8 \times 10^{-17}$emu for Sample A1 and A2, respectively. From the results of the measurements of particle radius, the average mole number per a grain particle is determined to be $N = 1.7 \pm 1.2 \times 10^{11}$ and $N = 5.1 \pm 2.5 \times 10^{11}$ for Sample A1 and A2, respectively. In Figure 5.3 it is noted that the deviation of the H_S-value from the the theoretical value is observed in the temperature range just above the melting point of the ethanol (158.5K). According to the equation(4.10) H_S-value in this temperature range

should be $N\Delta\chi$-values as $H_S \sim 3.15 \times 10^{-2}$ tesla and $H_S \sim 2.45 \times 10^{-2}$ tesla for Sample A1 and A2, respectively, The detail of the deviation is discussed in Chapter 6.

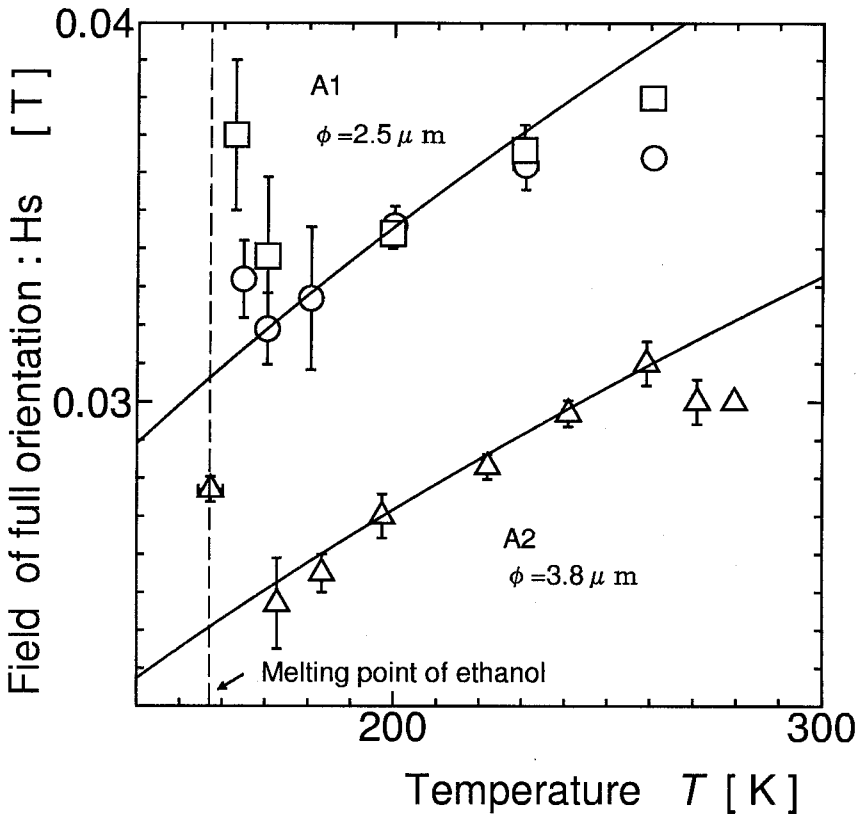

Figure 5.3: Relation between the temperature and field of full orientation H_S.

The temperature dependence on intrinsic $\Delta\chi$-value of the material should be evaluated in analyzing the measured H_S-T relation. It is known that the increase of the absolute $\Delta\chi$-value is as large as 2×10^{-5}emu/mol as the temperature decreases from 260K to 200K in the case of graphite, which is an exceptionally large temperature variation for diamagnetic anisotropy. However the H_S-variation due to this change is calculated to be less than 3%, which is smaller compared to the observed temperature variation. Hence the contribution

of the temperature variation of $\Delta\chi$-value to the H_S-T relation is considered to be negligibly small for the other materials.

The anisotropy of sheet silicates per chemical formula turned out to be approximately one order smaller than a Benzene molecule. For many of the sheet silicates, it is difficult to obtain a pure and large single crystal. This fact had prevented the study of diamagnetic anisotropy based on the conventional methods. The method of diamagnetic orientation described above enabled us to measure the anisotropy of the microcrystal for the first time, which serves as the method to accumulate the data of diamagnetic anisotropy.

5.2 Contribution of Magnetic Ions

The chemical composition of the natural samples measured in the work is shown in Table 5.1. The contribution of the magnetic ions contained in the samples as contamination should be evaluated quantitatively, in order to verify the diamagnetic $\Delta\chi$-values from the observed data. Before the experiment of the diamagnetic orientation, measurements of the magnetic susceptibility of the samples are carried out with the SQUID method for this purpose. For talc and phlogopite, the magnetization curves were detected which indicated diamagnetic feature with the magnetic ions above the detection limits of $< 0.5\times10^{-8}$emu/g. While paramagnetic ions of approximately 5×10^{-8}emu/g were detected for kaolinite and sericite samples. Two possible mechanisms are considered for the grain orientation caused by the paramagnetic ions. One possibility is due to the anisotropy of paramagnetic ions isolated in the crystal. The other possibility is the orientation due to the demagnetizing field caused by the geometrical anisotropy of the grains. For the former case, the contribution is estimated semi-quantitatively according to g-factors of the contaminated ions located at various M-sites presumed with the electric spin resonance. For the later case, the demagnetizing coefficient ΔN is assumed as $\Delta N = 0.92$ if the shape of the platy grain is assumed approximately as a spheroid with an aspect ratio of 0.05. The field intensity required to

realize the orientation can be estimated from the concentration of the magnetic ions in samples for both effects. The result of calculations shows that the required field intensity will be as high as 50 tesla for both effects in the case that the concentration of magnetic ions is 5×10^{-8}emu/g. Moreover, there is no correlation between the concentration of magnetic ions and observed field. It is concluded that the contribution of the magnetic ions to the grain orientation is negligible. The inclusion which has the spontaneous magnetization is another candidate which causes the magneto-orientation. However, the contribution of this effect is eliminated, since there are no detections of the spontaneous magnetization phase in the magnetization curves of the samples.

Table 5.1: Chemical composition of the natural samples.

	Kaolinite(D)	Lepidolite(F)	Talc (G)
SiO_2	42.98	53.61	61.62
MgO	0.01	0.46	32.28
Al_2O_3	37.61	16.32	0.30
TiO_2	0.50	—	0.02
CaO	0.35	0.58	0.24
MnO	—	0.73	< 0.01
Fe_2O^3	0.63	—	0.06
FeO	0.13	1.35	0.11
K_2O	0.44	10.90	0.07
Na_2O	0.32	0.94	0.05
F^-	—	7.92	—
Li_2O	—	6.55	—
H_2O^+	13.46	0.56	4.48
H_2O^-	0.46	0.68	0.01
Total	99.89	99.23	99.24

For the talc samples, the measurements were carried out for the aggregate in which the plane of the single-crystal grains was stacked on a certain direction. The magnetizations were obtained along the direction parallel and the perpendicular to the stacking direction. The difference of the two values is 1.1×10^{-5}emu/mol. This value is in accordance with the

value of $N\Delta\chi$ obtained with the grain orientation measurement and it is verified that the grain possesses the diamagnetic anisotropy which has the capacity to induce the magnetic orientation in the sheet silicates. According to these experimental results, the diamagnetic anisotropy per chemical species of the inorganic materials can be determined as an intrinsic physical quantity assigned to the individual species.

Chapter 6

Anomaly of H_S Values in the Viscous Medium

6.1 Experimental Results of Viscosity Effect

Figure 6.1 shows the deviation of experimental H_S-values with respect to the theoretical values which appeared in the H_S-T measurements of Figure 5.3. The origin of this large deviation could not be explained in terms of the thermal motions known for micron sized particles. One significant features in the low temperature region is that the viscosity of the suspension medium becomes extreamly large as seen in Figure 6.2. From the resemblance between the temperature dependence of the viscosity of ethanol and the dependence of H_S deviation, the effects of the viscosity can be inferred as the origin of the H_S-deviation. Figure 6.3 shows the relation between the viscosity and H_S for graphite grains measured at various temperatures.

6.2 $\langle m \rangle$-H Curves and Deviations of H_S

In order to confirm the effect of viscosity on H_S, the experiment was carried out using ethanol-glycerin mixture as the suspension medium which was described in §4.1.2. The typical examples of $\langle m \rangle$-H curves of Sample B and C at each viscosity are shown in Figures 6.4 and 6.5, respectively. In Figure 6.4, open and solid circles are the experimental

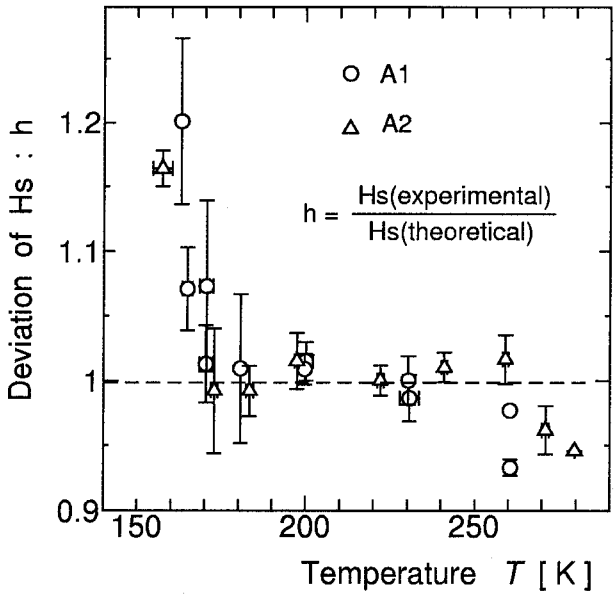

Figure 6.1: Deviation of H_S as the ratio of the experimental values for the theoretical values on graphite.

$\langle m \rangle$-values. In Figure 6.5, those values are indicated with open circles. The curves in these Figures are the theoretical values calculated based on equation(4.4). The measured viscosity dependence of the H_S is shown in Figure 6.6 for sample A and B. The H_S-values are constant at viscosity below $\eta = 1000$cp following the relation of equation(4.10). However the H_S-values show a significant increase from 100 to 700 gauss as the viscosity changed from 1700 cp to maximum value of 11250cp. Comparing the values of H_S in the viscous medium with those in non-viscous medium, the value of H_S at viscosity $\eta = 1700$cp is about twice as larger and the value at maximum viscosity $\eta = 11250$cp is about four times larger than the case with a viscosity of ethanol at room temperature.

The open triangles of Figure 6.6 are the data obtained from the deviation observed in the H_S-T measurements. It is seen that the viscosity at which the H_S deviation begins is below

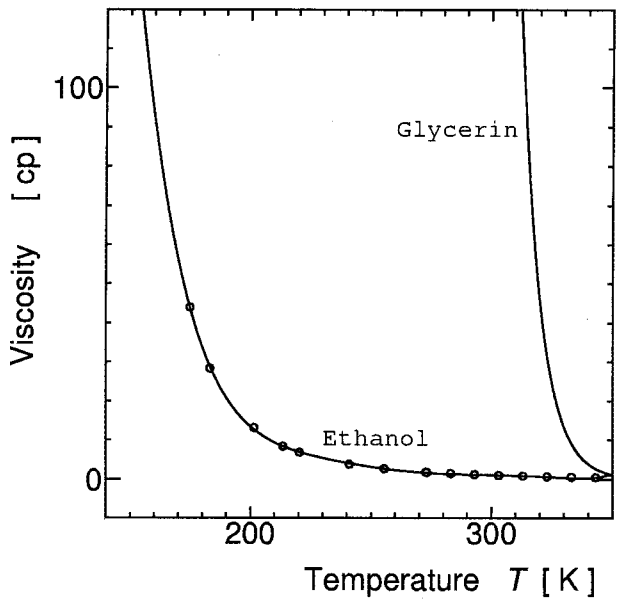

Figure 6.2: Viscosity of ethanol and glycerin as functions of temperature (JSME Data Book : Thermophysical Properties of Fluids 1983).

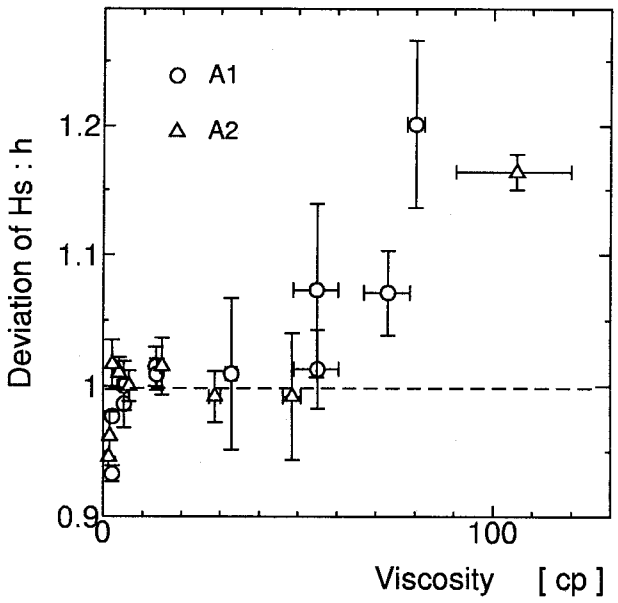

Figure 6.3: Viscosity dependence of H_S-values for graphite grains.

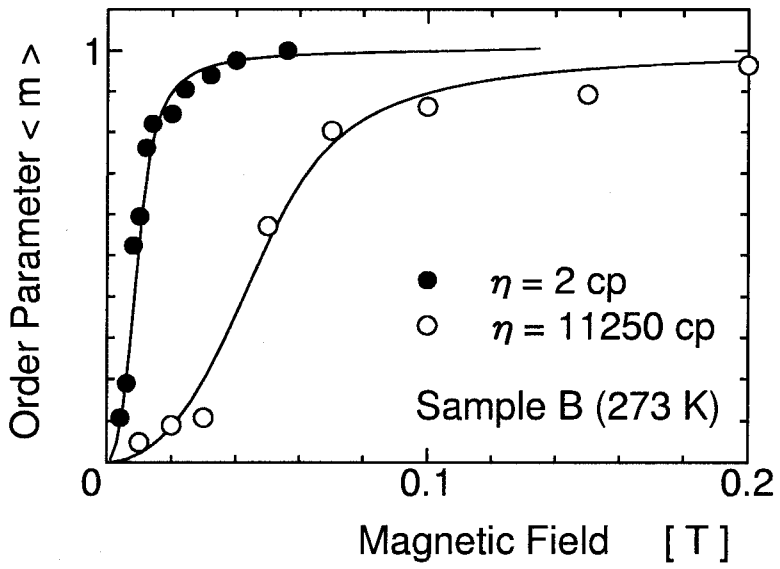

Figure 6.4: Typical examples of $\langle m \rangle$-H curves at low and high viscosity on Sample B.

η = 100cp which is one order of magnitude smaller than that of the H_S-η measurement. The high viscosity is considered to affect only the relaxation time required to saturate the orientation. Indeed, in the case of the high viscous medium the relaxation time is longer than the case of the low viscous medium. Therefore the judgment of the completion of the relaxation requires a long time interval. Hence the measurement of the experimental order parameter during relaxation process may lead the deviation of the field strength H_S. However, this apprehension can be excluded because the behavior of the individual $\langle m \rangle$-H curve indicates the feature of the thermal equilibrium expressed by equation(4.4) even in the high viscous medium. Moreover, if an error of judgment had made, the H_S-value would

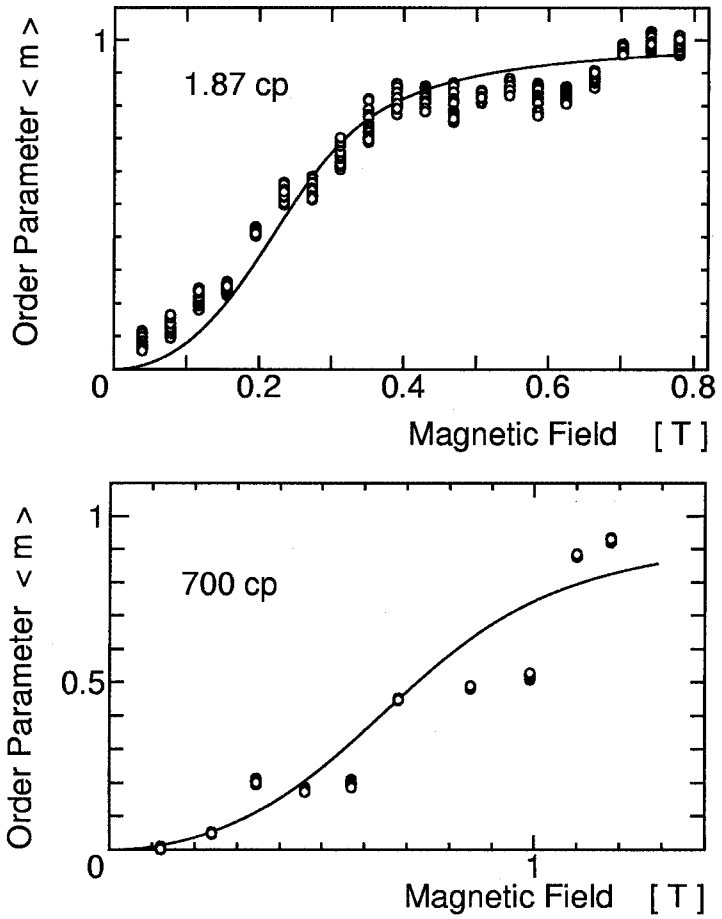

Figure 6.5: Typical examples of $\langle m \rangle$-H curves of Sample C3 at low viscosity.

be smaller.

6.3 Effects of Size Distribution on the Viscous Anomaly

As mentioned in the above section, H_S-value is dependent on three parameters: the temperature of the grain and the medium, T, mole number of the grain (proportional to the grain size), N, and the intrinsic anisotropy of the grain material, $\Delta\chi$. In the conventional picture of Brownian motion, the viscosity of the medium does not contribute to the energy state of the particle. The viscosity is considered to affect the relaxation of the particle motion as mentioned above. Hence the term of viscosity do not appear in the equations

of $\langle m \rangle$ and H_S, which are also based on the conventional picture of Brownian motion. As mentioned before the equations are based on the balance of field-induced anisotropic energy and thermal agitation energy. It is noted that the observed $\langle m \rangle$-H relation shows good agreement with the theoretical curve of equation(4.4) even in the high viscosity region. This indicates that the orientation mechanism assumed in Chapter 4 is effective in the high viscous region. Consequently the effective values of the three parameters $(N, \Delta\chi, T)$ should be altered considerably, in order to account for the large discrepancy of the observed H_S-values.

It is obvious that the intrinsic diamagnetic susceptibility of the particles is not altered by the viscosity of the medium. The origin of this deviation of the observed H_S-values, without changes of thermal equilibrium condition, can be interpreted as the change of the effective grain size N or the effective temperature T. In this thesis the author will discuss the problem in terms of the change of the effective grain size, since the grains used in the actual measurement had a size distribution of standard deviation $\sigma \simeq 50\%$ with respect to the average values.

The cross-over features

In the calculation of the H_S curves the single size of the particles is assumed in equation(4.3) and equation(4.4). As mentioned above, however, there are various sizes of particles in the actual sample suspensions. It is expected that the observed $\langle m \rangle$-H curves deviate from the theoretical curve by this size effect. This deviation often appeared in the $\langle m \rangle$-H curves obtained from the experiments in the low viscous mediums, in which the experimental values are larger than the theoretical values in the low field region while in the high field region the experimental values are smaller than the theoretical values. The example of $\langle m \rangle$-H curve on graphite sample showing this feature is given in Figure 6.7. This feature is hereafter referred to as the *cross-over feature*. This feature has been

also found in the earlier literatures on the diamagnetic orientation (e.g. Yamagishi et al. 1989). The results of the experiments showed that the *cross-over feature* in the high viscous medium is small and the experimental values are in good agreement with the theoretical curve.

Provided that the sample particles possess some amount of size distribution, the $\langle m \rangle$-H curves in the low viscous medium can be expressed by the superposition of many $\langle m \rangle$-H curves of particles which have different sizes. The situation is such as shown in Figure 6.8. Consequently the above results may be explained by the following mechanisms:

1. In the low viscous medium it is expected that the large particles orient first when the applied field is small and the smaller particles orient gradually as the applied field increases, and at last all particles complete the orientation.

2. In the high viscous medium it is expected that the size range of the mobile particles becomes smaller because the effect of the viscous resistance becomes large for the larger-sized grains. Eventually, only small particles which are not affected by the viscosity resistance can orient selectively.

Consequently the apparent H_S will increase above a certain viscosity. The *cross-over feature* becomes small when the experiments are preformed using the uniform-sized particles. The advanced experiments on sample group-C were performed to examine this assumption. The red-blood-cell (R.B.C.) is referred as the example of the narrow size distribution (Mizuno 1994). The $\langle m \rangle$-H curves are shown in Figure 6.9.

Quality of fitting

In order to evaluate the deviation of the experimental values from the theoretical $\langle m \rangle$-H curves in the *cross-over features*, it is convenient to adopt the sum of the least-square as the quality of fitting. The quality of fitting, QF, is defined as the value of which the residual

divided by the degree of freedom of the fitting:

$$QF = \frac{1}{n}\sum_i (m_{the_i} - m_i)^2 \quad , \tag{6.1}$$

where n is the degree of freedom of the fitting parameters, m_{the_i} is the calculated order parameter, m_i is the measured order parameter at i-th field. In this definition, the smaller value of QF means that the deviation of the measured data from the theoretical data is small.

The calculated QF values are shown in Table 6.1. The value of R.B.C., is found to be nearly two orders of magnitudes smaller than that of other samples.

Table 6.1: The viscosity dependence of the quality of fitting.

Sample	viscosity [cp]	Quality of Fitting
C1	1.9	$2.90 \times 10^{-3} \pm 7.0 \times 10^{-4}$
	700	$6.28 \times 10^{-3} \pm 1.0 \times 10^{-2}$
C2	1.9	$2.20 \times 10^{-2} \pm 1.6 \times 10^{-2}$
	700	$1.16 \times 10^{-2} \pm 8.0 \times 10^{-3}$
C3	1.9	$1.45 \times 10^{-2} \pm 1.1 \times 10^{-2}$
	700	$2.24 \times 10^{-2} \pm 1.3 \times 10^{-2}$
R.B.C.	~ 2	$8.14 \times 10^{-4} \pm 4.0 \times 10^{-4}$

Evaluation of size distributions

In order to evaluate the relation between the width of the size distribution and the quality of fitting, the size distributions are obtained through the imaging processing. The SEM images are processed into binary colored images with NIH image package in order to distinguish the particles and the background. The grain size is estimated with counting

the pixel number of the particles on the images. Here the pixel number of the maximum axis length represents the grain size. The histograms of the size distribution of samples are shown in Figure 6.10. The total sampling numbers of the particles are 200, 134, and 372 for the Samples C1, C2 and C3, respectively. The average sizes of the samples can be defined as 28.9μm, 0.38μm and 3.8μm. All samples have the Gaussian-like distributions, and their standard deviations are 29μm, 0.19μm and 2.3μm. The shapes of each distribution are plotted in Figure 6.11 by the normalized radius. Table 6.2 shows the parameters of each normalized distribution. It is seen that Samples C2 and C3 have similar distribution, but Sample C1 and R.B.C. are considerably narrower.

Table 6.2: Parameters of the normalized distribution for samples.

Sample	Gaussian center	Half width	Ref.
C1	0.557	0.543	this work
C2	0.870	0.588	-
C3	0.791	0.603	-
R.B.C.	1.020	0.216	Mizuno 1994

Size distribution effect on QF

The relation between the values of QF and the half width of the distribution for low viscous medium ($\lesssim$700cp) is plotted in Figure 6.12. From the reanalyzed results on R.B.C. the QF-value turned out to be $QF = 8.14 \times 10^{-4} \pm 4.0 \times 10^{-4}$. For Samples C1-C3 the QF-values lie in the range from 4.6×10^{-3} to 1.7×10^{-2}. It is clearly seen that the QF-value increases with the half width of size distribution, indicating that the *cross-over feature* is caused by the large distribution of grain size.

6.4 Discussion

The above result indicates that the origin of such anomalies of H_S in viscous medium may be explained in terms of the size distribution of particles in the suspension. As mentioned before the *cross-over feature* was relatively small in the high viscosity region. The fact that the H_S-values were enormously large in this region indicates that only the small-sized grains were able to cause orientation. It can be interpreted that the larger-sized particles in a wide distribution are limited to move by the viscous resistance force in the high viscous medium. The thermal equilibrium of moving particles are preserved in these ensembles. Consequently the *cross-over feature* is reduced as the viscosity becomes high (Figure 5.1). If this is the case, the upper limit of the mobile size of the particle should exist at a certain value of viscosity. So far the orientation of micro-crystal is understood only with the energy balance between the field-induced energy of the particles, U, and the thermal agitation energy of the system, k_BT. The present result, however, suggests that the effect of the viscous resistance should be taken into account besides the conventional energy balance of the diamagnetic orientation: U vs. k_BT in the high viscosity medium. The origin of the viscous resistance is unsolved yet.

If only a part of the particles is oriented in the viscous medium, the absolute value of the experimental order parameter (i.e. the laser intensity) must have the dependence on the viscosity. This is because the cross section which intercepts the laser beam flux is related to the size of mobile particles. In order to examine this effect, the experiment should be carried out under conditions where the viscosity and the concentration of the sample suspension are controlled precisely. Since the viscosity of the medium has a direct relation with the temperature, the viscosity control can be realized by the control of the temperature. The outline of the developing setup for measuring in low temperature for this purpose is given in Appendix B. Also the reproducing of the *cross-over feature* of the

$\langle m \rangle$-H curve with a numerical calculation is required to prove the *cross-over feature*.

It is seen in Figure 6.6 the inclination of the deviation of H_S is different between the Samples A and B. For Sample A the deviation of H_S begins at viscosity about 100 cp. For Sample B it begins at viscosity about 1000 cp. This feature cannot be explained in terms of the macroscopic viscosity alone. The difference of the two experiments is the temperature of the medium. The experiments using Sample A were performed in low temperature. Therefore, the H_S-deviation in Sample A may be due to some microscopic molecular interaction which may become significant just above the melting point of the medium. That is, the cause of viscous resistance mentioned above cannot be expressed in terms of the macroscopic viscous coefficient.

In addition the viscous resistance may also increase the effective temperature, T, of $H_S = \sqrt{15k_BT/N\Delta\chi}$, which is another possibility to cause the viscous effect. This possibility should also be examined through further investigation.

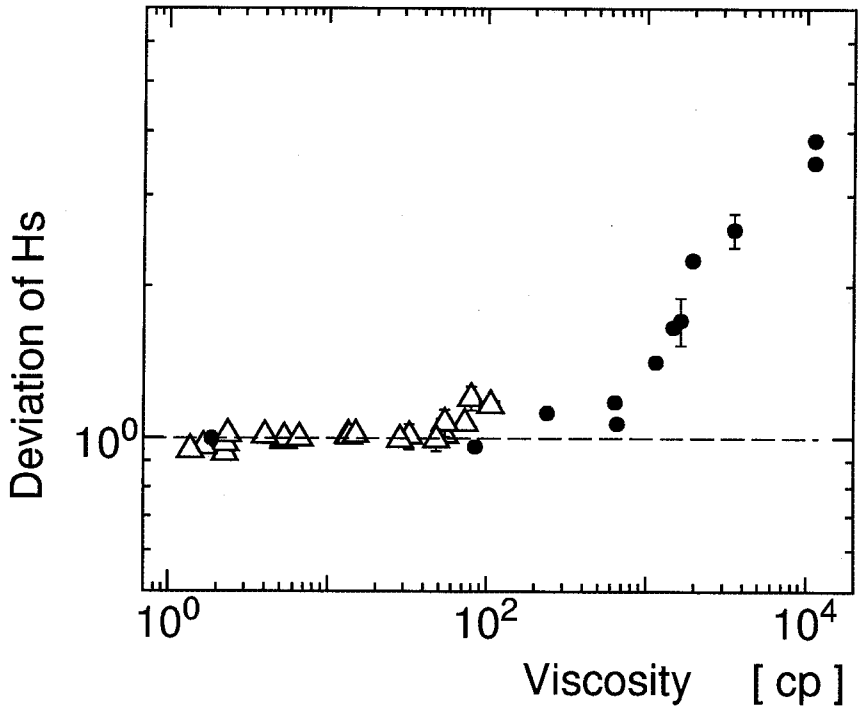

Figure 6.6: The viscosity dependence on H_S for graphite grains. The solid circles and the open triangles indicate the experimental data of Samples A and B, respectively.

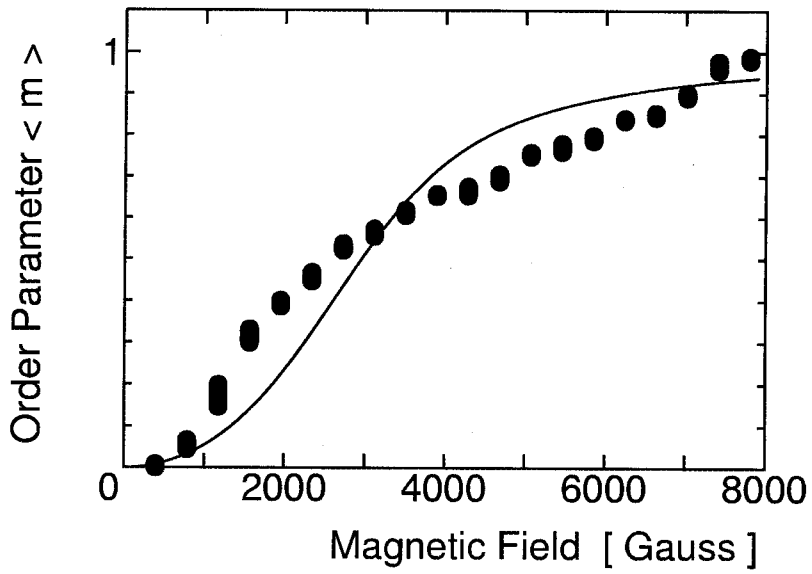

Figure 6.7: The example of $\langle m \rangle$-H curve with the *cross-over feature* in low viscous medium.

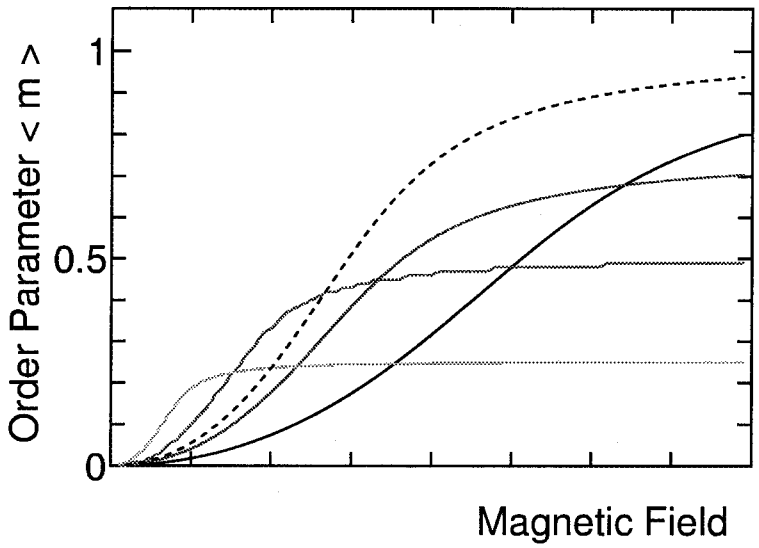

Figure 6.8: The schematic representation of the $\langle m \rangle$-H curve expressed by the superposition of various $\langle m \rangle$-H curves with different size ensembles. The solid curves are individual $\langle m \rangle$-H curves of different size ensembles and the dashed curve is the $\langle m \rangle$-H relation of an uniform-sized ensemble.

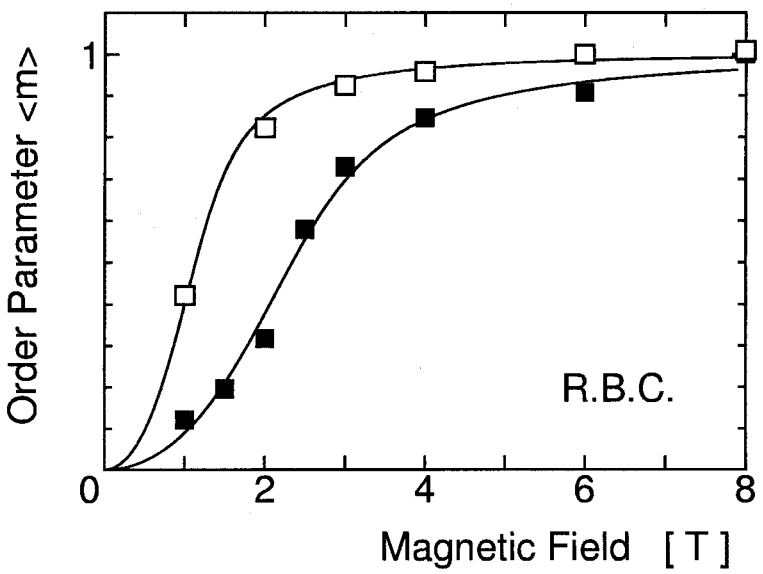

Figure 6.9: The $\langle m \rangle$-H relation on R.B.C. from the data of Mizuno 1994. This is the example of $\langle m \rangle$-H curves without the *cross-over feature* in low viscous medium.

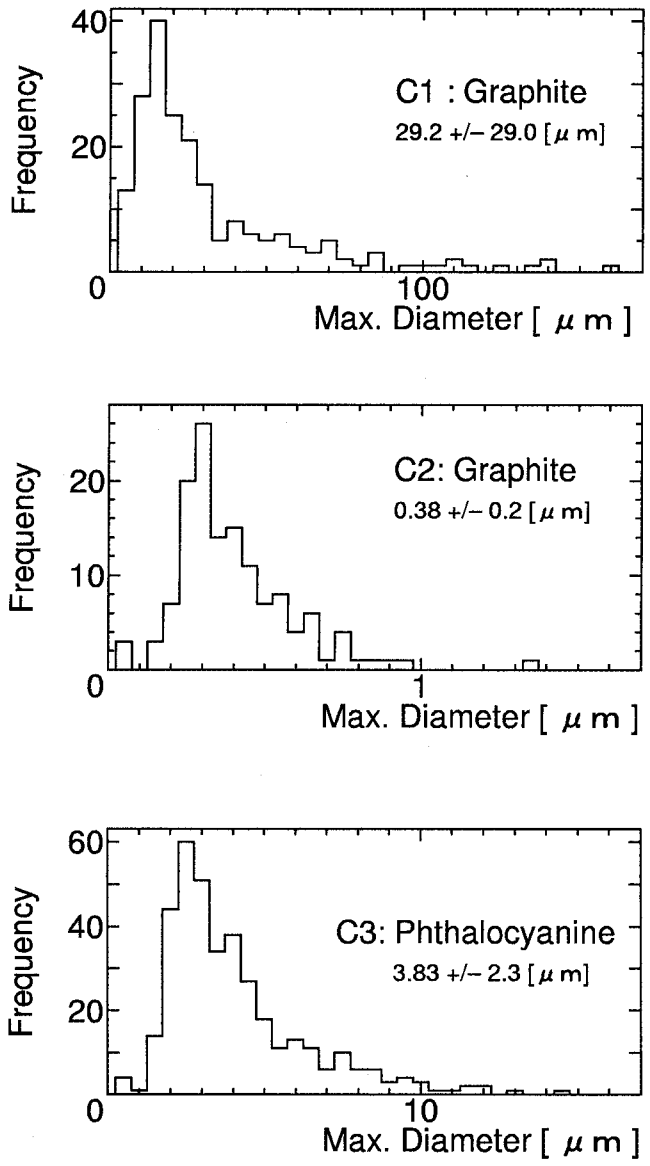

Figure 6.10: The histogram of size distribution of samples particle labeled C1-C3.

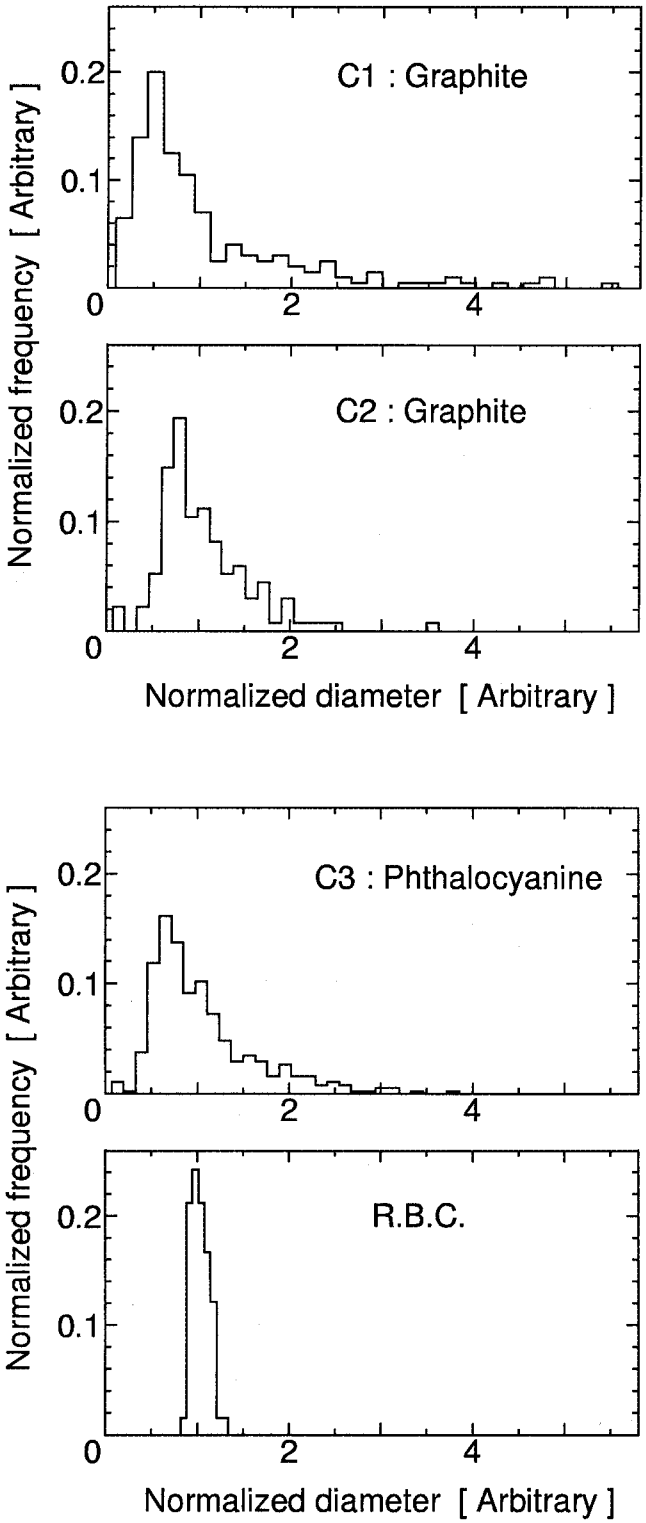

Figure 6.11: Normalized distributions of Samples labeled C1-C3 and R.B.C.

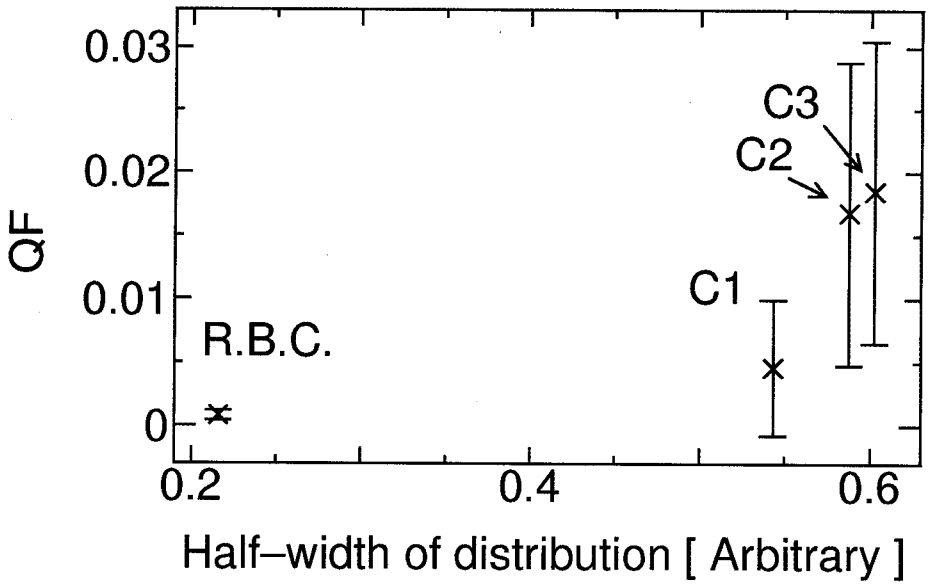

Figure 6.12: The relation between the half width of the distribution and the quality of fitting.

Chapter 7

Application to Astrophysics

7.1 Possibility of Diamagnetic Orientation in Interstellar Environment

As described in Chapter 3, the observation and analysis of magnetic field in nature have revealed a number of novel phenomena especially in the field of earth and space sciences. For example, the paleomagnetic record over the past billion years of the earth surface has confirmed the mechanism of plate-tectonics, which dominates the evolution of the earth curst. The studies on the interactions between the earth's magneto-sphere and solar wind which causes of the aurora in the polar zone, have revealed the complex behavior of the charged particles surrounding the earth. Various phenomena caused by the magnetic field at the sun surface, such as sun-spots, flares or prominences have provided useful information to investigate the nature of the solar activity. The magnetic field in the interstellar space restricts the motion of interstellar matters and consequently dominates the early stages of star and planet evolution. It is noted that the origin of the observed magnetic phenomena has been considered mainly on the effect of the electron spins in solids as well as that of the charged particles which are in Lorenz motion. Therefore the candidates of magnetically-active materials which hold a very small portion among the total materials in the Universe, were limited to the magnetic elements and the charged particles. More than 95% atomic percent of the solid materials are considered to be non-magnetic, according to

the cosmic elemental abundance. The results of the previous experiments indicate that the major components of the cosmic solid-phase, including the bulk earth materials, possess the efficiency of magneto-orientation to some extent. Hence various ordering phenomena in the Universe should be reconsidered from this point of view, even though their magnetic efficiency may be considerably smaller compared to the "magnetically-active materials".

The mechanism based on the conditions of the diffuse regions, is applied to the dense region as well. In the dense region where the interstellar extinction is large, such as in the molecular-cloud core, the polarimetric observation in visible wavelength is not a powerful tool to measure the magnetic field. Instead, the observation of polarization in near infrared wavelength is considered to provide the effective manner to measure the magnetic field. The polarization of this wavelength is also attributed to the alignment of grain as mentioned above. Figure 7.1 shows the typical results of the infrared observation carried out for the star formation region (Tamura et al. 1987). Figure 7.1(a) shows the direction of polarization of individual stars; the contour shows the intensity of the infrared radiation of the molecular cloud and the straight lines superposed on the contour map show the degree and the direction of polarization of the star. The direction of the magnetic field is aligned in order if one assumes that the direction of infrared polarization is parallel to the magnetic field. The Galactic field of the surrounding area is usually observed to be parallel to the polarization in the clouds. Due to the fact that the direction of elongation of the cloud is perpendicular to the magnetic field, it is generally inferred that the cloud is formed by compression in the direction parallel to the magnetic field due to Lorentz motion. This situation is illustrated in Figure 7.1(b).

It is noted that the DG theory is operative only for the region of non-thermal equilibrium system of the diffuse clouds, because the fundamental process of the DG theory is the rotation of grains due to the gas-grain collisions as is reviewed in Chapter 3. Since the collision between the gas particles and grains occurs more frequently in the dense region than in

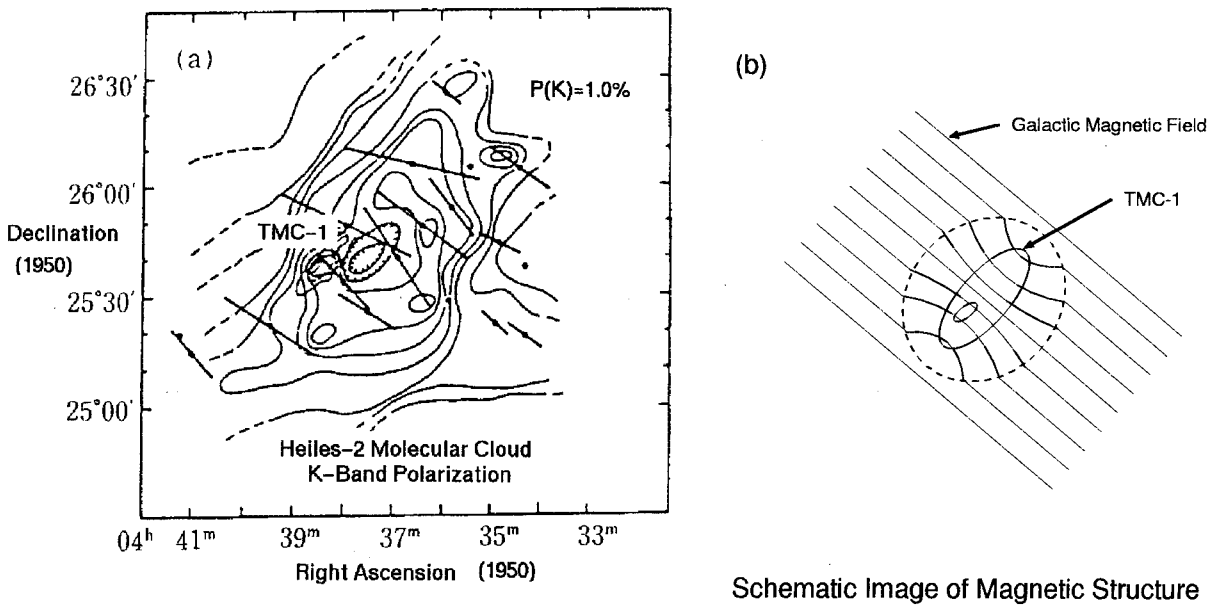

Figure 7.1: (a) The polarization of near infrared observation of Taurus Molecular Could-1 (TMC-1) and (b) the schematic image of the magnetic structure. (Tamura et al. 1987)

the diffuse regions, it is expected that a quasi-thermal equilibrium condition between grain and gas molecules is realized in this region. Therefore, the estimated magnetic field based on the DG theory for this region still leaves room for discussion (e.g. Whittet 1992).

7.2 Conditions for Diamagnetic Orientation in Nature

The field necessary to achieve the diamagnetic orientation is compiled in Figure 7.2 for various regions of the Universe. The $N - H_S$ relations of equation(4.10) are calculated for natural materials of various intrinsic $\Delta\chi$ values and at various temperatures. It was suggested that the relatively large grains ($\geq 100\mu$m) show orientation by the terrestrial field.

For the diffuse interstellar region, the field of orientation is required to be approximately $H_S = 100$G according to the estimation based on the experimental data of Figure 5.3. The diamagnetic anisotropy-energy is too small to cause direct grain alignment in this region.

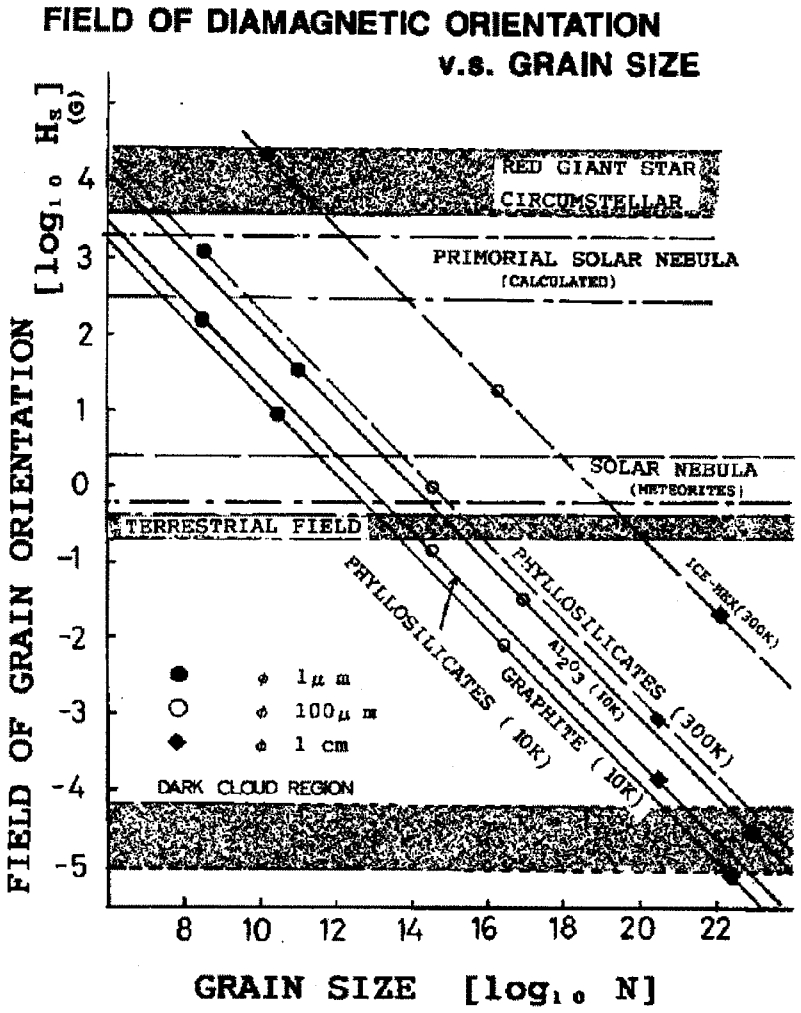

Figure 7.2: The limitation of diamagnetic orientation in the interstellar environment.

It is noted that the Galactic-field-induced energy of the ferromagnetic or paramagnetic ions was also recognized to be too small compared to the thermal energy to realize direct grain orientation is in the diffuse condition (Spitzer and Tukey 1951). Consequently an *indirect* multi-stage model based on paramagnetic relaxation (the DG theory) was introduced, based on the well-established paramagnetic properties of solid state physics in the low temperature region. In the same manner the results of diamagnetic anisotropy described in the previous chapters may serve as a basis to construct a multi-stage model based on diamagnetic properties, if one considers the diamagnetic anisotropy as the alternative driving force of interstellar grain-alignment instead of the paramagnetic properties.

The ambiguity of the DG theory lies in the actual content of the magnetic phases. The electron spins of the grains may form magnetic phases other than the assumed phases of the DG theory. For example, the mechanism based on the DG theory is not operational if the spin consists of the ordered ferro-, ferri- or anti-ferro-manganetic phases. There are no intense investigations so far to exclude these phases in the interstellar environment. Hence the actual state of the magnetic-phase of the grain is rather ambiguous for evaluating the efficiency of the DG theory at this moment. The super-paramagnetic structure, being assumed as a break through to the problem of the low abundance of magnetic elements, is also an irregular structure to be found generally in the interstellar region. Moreover the improved the DG theories are based on assumptions of extreme conditions such as the existence of the supra-thermal rotation, which cannot be examined either from experiments or by astronomical observations.

A mechanism assuming an interaction between the diamagnetic properties of the grain and the Galactic field will be free from such uncertainty on magnetic phases. That is, the results of the experiments mentioned in previous chapters indicated that most of all the interstellar materials may possess the rotational-efficiency of diamagnetic orientation. Formerly the efficiency was recognized only for the graphite grains (Cayrel and Schatzman

1954; Greenberg 1969; Purcell 1969). Hence it may be worthwhile to reconsider the possibility of the ordering mechanism based on diamagnetic anisotropy, which may be a more convincing characteristics for the interstellar grains.

In the case of diamagnetic materials, however, the magnetic properties are still unknown especially in the low temperature region, and the possibility of new diamagnetic effects in the region cannot be erased at the moment. For example, the effective $\Delta\chi$-value of diamagnetic materials may be enhanced drastically, as seen in the case of graphite which probably reduces the field of orientation considerably. In this sense, the experimental studies are required on diamagnetic materials in the low temperature region in terms of the method described in Chapter 3.

In dense clouds, the temperature is expected to be lower ($T \sim 10$K) and the grain size is expected to be larger compared to the diffuse cloud conditions. These two characteristics reduce the field of full orientation described in equation(4.10). As mentioned above, the DG theory is only operative in the non-thermal equilibrium environment. In the dense regions where the thermal equilibrium is realized, the grain orientation caused by the balance between field-induced energy and the thermal energy described in Chapter 2 is more likely to happen. According to the estimation of Chihara et al. (1998) the field of full orientation in the proto-planetary environment with a temperature of $T \sim 10$K, is calculated by the use of equation(5.3) to be 1.7mT using the average size of the primordial-solar graphite grains isolated from Murchison meteorite which is 4.5μm in diameter (Amari et al. 1994). Magnetic orientation may occur in this region, since the field in the primordial planetary system is estimated to be as large as 0.1mT according to the estimation of the residual magnetization of meteorites.

As mentioned before the magnetic field plays a vital role on the formation of stars as well as on the evolution of its planetary system according to the theoretical studies. The molecular-cloud cores compressed by the magnetic field (Figure 3.3) are considered to form

the dust disks in their interior, which finally evolve to the planetary systems. More recently it was concluded that the bipolar flow ejected from the primitive stars, commonly observed in the star formation region, is controlled by the magnetic field close to the primitive star, and its extension is connected to the interstellar magnetic field. This mechanism is considered to be vital for the primitive star to diminish its large angular momentum and to evolve to a main sequence star with normal angular momentum. It is noted that the spatial resolution of the method 4 mentioned in §3.1, which has the highest resolution of the order of 10000AU [1] (for TMC), is not high enough to observe the theoretically predicted magnetic-field structures mentioned above.

The recent observation reveals that the circumstellar disk of the size of 100AU is detectable with the spatial resolution as high as 10AU (Lagage and Pantin 1994). The polarimetric observation with a similar spatial resolution will provide the information of the local field structure. Thus the observational examination of the field structure of primordial planetary systems predicted by the theoretical works would become possible in the near future. It is considered that the primordial systems are also in a quasi-equilibrium condition where the diamagnetic orientation serves as an effective mechanism to analyse the grain alignment data rather than the DG theory, as is the case of the molecular clouds.

Finally the experimental method on grain orientation described in Chapter 2 can be applied to an experimental examination of the mechanism of star-light polarization. In order to examine the theoretically derived relation between the star-light and the degree of grain orientation, it is necessary to perform a well controlled experiment. Various parameters of the grains, such as the size, geometry (e.g. radius/length ratio of a rod sample), dielectric function, substance of the grain, degree of orientation and so on, are considered to affect the polarization. These parameters can be easily controlled experientially by choosing the

[1] AU (Astronomical Unit) : AU represents the distance between the Sun and the Earth. 1AU $\sim 1.5 \times 10^{11}$m

grain material as well as by controlling the $\langle m \rangle$-H relation. The dependence of the polarization due to the optical wavelength as well as the temperature of the medium may also be examined.

Chapter 8

Conclusions

The experimental results, which were analysed with the conventional analytical procedure on the diamagnetic orientation of inorganic micro-crystals, have revealed that the orientation efficiency of a grain is dependent on three parameters: the temperature of the grain T, the mole number corresponding to the size of the grain N and the intrinsic anisotropic susceptibility of the material $\Delta\chi$. The origin of the $\Delta\chi$-values can be attributed to the anisotropies of the bond directions of the individual crystal. The results indicate that most of all the diamagnetic crystals posses the efficiency of magnetic rotation.

In the actual measurement the sample ensembles have various distributions on particle size. The effect of the sample size distribution is appeared as the *cross-over feature* in the low viscous region. The wide distribution can be considered as the cause of the H_S-deviation in the high viscous region. In the low viscous medium, the larger particles which have larger field-induced energy orient prior to the smaller particles. If the sample ensemble has a size distribution, the *cross-over feature* is observed because the average size of the particles which can be oriented differs according to the field strengths. In the high viscous medium, the larger particles are restricted to move by the viscous resistance force. Consequently the value of H_S increases because the only smaller particles are responsible for the orientation selectively. A good agreement with the observed and theoretical $\langle m \rangle$-H curves even in high viscous medium is explained with the interpretation that the thermal

equilibrium is preserved in the ensemble of small mobile particles.

The possibility of the diamagnetic orientation is discussed in the interstellar environment. Since the Galactic magnetic field is the only factor which may align the grain particles and is omnipresent through the Galaxy, it is generally believed that the Galactic magnetic field is the origin of the grain alignment. The elemental abundance of the magnetic ions, however, gives a severe constraint to the conventional mechanism of the magnetic ordering of the grain. The diamagnetic properties of interstellar materials may be reconsidered as a possible driving force of the grain alignment. The applicable region for diamagnetic orientation can be assumed based on the N-H_S relation obtained from the experiments. Since the efficiency of the orientation depends on the temperature and the size of the grain, it is concluded that the diamagnetic orientation can be considered as a candidate of the mechanism of interstellar grain alignment in the dense region such as molecular cloud core and proto planetary disk where star and planet formation take place.

Acknowledgments

I wish express the grate thanks to Professor T. Sunamura for the many advice on this work, continuous encouragements and thorough correction of the manuscript.

I wish express the special thanks to Dr. C. Uyeda who had first suggested this theme to me and many useful discussions on this work and continuous encouragement.

I also wish express the thanks to Professor J. Matsuda for his suggestion on the analytical procedure at the early stage of this work. I also like to express my thanks to Mr. T. Komatsu for his great support on the experiments on the viscosity effect. I also wish express the thanks to Dr. K. Hayasida in X-ray astrophysical group for his permitting me to change the thema halfway of the Doctor course. I would apologize to him for my leaving the previous work half done.

Dr. M. Furusawa in Japan Advanced Institute of Science and Technology is also thanked for his helpful advice on operating the SIMS to estimate the purity of the samples. I would also like to express my thanks to Mr. S. Tachibana, Mr. T. Hattori, Mr. K. Okita and all members of the Geology group of Dept. of Earth and Space Science.

Finally, I thank my family and especially the late my father for great encouragement and support.

Bibliography

[1] Amari S., Lewis R.S, Anders E., 1994, Geo.Cosmochem.Acta, 58, 459-470

[2] Axon D.J., Ellis R.S, 1976, Mon.Not.Roy.Astron.Soc., 177, 499-511

[3] Beams J.W., 1932, Rev.Mod.Phys., 4, 133

[4] Birle J., Gibbs G.V., Moore P.B., Smith J.V., 1968, Am.Mineral, 53, 807-824

[5] Born M., 1918, Ann.Phys., 55, 177

[6] Buckingham A.D., Polple J.A., 1956, Proc.Phys.Soc., 69, 1133

[7] Cayrel R., Scheatzman E., 1954, Ann.Astrophys. 17, 555

[8] Chihara H., Uyeda C., Tsuchiyama A., Yamanaka T., 1998, Publ.Astron.Soc.Jpn., 50, 149-154

[9] Chihara H., Okamura T., Uyeda C., 1998, J.Magn.Magn.Matter, 177-181, 1455-1456

[10] Chihara H. and Uyeda C., 1998, Recent Research Development in Applied Physics, in press

[11] Cotton A., Mouton H., 1907, Compt.Rend., 145, 229

[12] Davis L., Greenstein J.L., 1951, Astrophys.J, 114, 206-241

[13] Greenberg J.M., 1969, Physica 41, 92-99

[14] Greenberg J.M., 1978, *Cosmic Dust* (Wiley & Sons, NewYork), 187-294

[15] Gupta C., 1983, *Diamagnetism, in Landort Börnstein New series II/16-9*, (Springer, Berlin), p.445

[16] Heiles C., 1987, Interstellar Processes, (Reidel, Dordrecht), 171-194

[17] Horau J., Lumbroso N., Pacult A., 1956, Compt.Rend., 242, 5050

[18] Krishnann K. S and Banerjee S., 1933, Phil. Trans. Roy. Soc. London, A231, 326-342

[19] Lagage P.O., Pantin E., 1994, Nature, 369, 628-630

[20] Langevin M. P., 1910, C.R.Acad.Sci.Paris, 151, 475

[21] Lazarian A., 1995, Astrophys.J, 453, 229-237

[22] Londsdale K., 1949, Nature, 164, 101

[23] Maret G., Schickfs M.V., Mayer A., Dransfeld K., 1975, Phys.Rev.Lett., 35, 397-400

[24] Maret G., Dransfeld K., 1977, Physica B, 86-88, 1077-1083

[25] Maret G., Torbet J., Senechal E., Domard A., Rinaudo M., Milas H., 1979, *Nonlinear behavior of molecules, Atoms and Ions in Electric, Magnetic and Electromagnetic Fields*, ed. L.Neel (Elsevier, Amsterdam), p.477

[26] Maret G., Dransfeld K., 1985, *Strong and Ultrastrong Magnetic Fields* (Springer-Velag, Berlin) 143-204

[27] Melville D., Paul F., Roath S., 1975, Nature, 255, 706

[28] Mizuno T., 1994, M.Sc. Thesis, Osaka University, 39pp

[29] Neininger N., 1992, Astron. and Astrophys, 263, 30-36

[30] Owen C.S., 1978, Biophys. J., 22, 171-178

[31] Pauling L., 1936, J.Chem.Phys. ,4, 672-678

[32] Pauling L., 1979, Proc.Natl.Acad.Sci., 76, 2293-2295

[33] Peterlin A. Stuart H.A., 1939, Z.Physik., 112, 1 and 129

[34] Purcell E.M. 1969, Physica, 41, 100-127

[35] Purcell E.M. 1979, Astrophys.J, 231, 404-416

[36] Rao S.R., Leela M., 1953 Current Sci., 3. 72

[37] Sazaki G., Yoshida E., Komatsu H., Nakada T., Miyashita S., Watanabe K., 1997, J.Crystal Growth, 173, 231-234

[38] Sénéchal E., Maret G., Dransfeld K., 1980, Int.J.Biol.Macromol., 2. 256

[39] Simonsen W.J., Gill S.J., 1974, Rev.Sci.Instrum., 45, 1425-1426

[40] Spitzer L.Jr., Tukey J.W., 1951, Astrophys.J, 114, 187-205

[41] Spitzer L.Jr, 1978, *Physical Processes in the Interstellar Medium*, (Wiley & Sons, New York), 171-190

[42] Spitzer L.Jr., McGlynn T.A., 1979, Astrophys.J, 231, 417-424

[43] Tamura M., Nagata T., Sato S., Tanaka M., 1987, Mon.Not.Roy.Astron.Soc., 224, 413-423

[44] The Japan Society of Mechanical Engineers, 1983, *JSME Data Book : Thermophysical Properties of Fluids*, (JSME, Tokyo), 547pp

[45] Troland T.H , 1990, *Galactic and Interstellar Magnetic Field*, IAU, 293-300

[46] Twersky V., 1969, J. Opt.Soc.Am., 60, 1084-1093

[47] Uyeda C., Takeuchi T., Yamagishi A., 1991, J. Phys. Soc. Jpn, 60, 3234-3237

[48] Uyeda C., Takeuchi T., Yamagishi A., Date M., 1992, Physica B, 177, 519-523

[49] Uyeda C., Tsuchiyama A., Yamanaka T., Date M., 1993, Phys.Chem.Minerals, 20, 82-85

[50] Uyeda C., Takeuchi T., Yamagishi A., Tsuchiyama A.,Yamanaka T., Date M., 1993, Phys.Chem.Minerals, 20, 369-374

[51] Uyeda C., 1993, Phys Chem Minerals, 20, 77-81

[52] Uyeda C., Makoshi Y., Miyako Y., Chihara H., Yamanaka T., Date M., 1995, J.Magn.Magn.Matter, 140-144, 2181-2182

[53] Uyeda C., Chihara H., Okita K., 1998, Physica B, 245-247, 171-174

[54] Verscheuur G.L. , 1969, Astrophys.J, 155, L155-L158

[55] Whittet D.C.B., 1992, *Dust in the Galactic Environment*, (IOP, New York), 83-114

[56] Whckoff R.W.G., 1948, *Crystal Structures*, (Interscience, NewYork)

[57] Yamagishi A., Nagao E., Date M., 1984, J.Phys.Soc.Jpn., 53, 928-931

[58] Yamagishi A., Takeuchi T., Higashi T., Date M., 1989, J.Phys.Soc.Jpn., 58, 2280-2283

[59] Yamagishi A., Takeuchi T., Higashi T., Date M., 1990, Physica B, 164, 222-228

[60] Yamagishi A., 1990, J.Magn.Magn.Matter, 90-91, 43-46

[61] Zweibel E.G., 1987, *Interstellar Processes*, (Reidel, Dordrecht), 195-221

Appendix A

Analysis Procedure on Microsoft Windows

The part of the source code for $\langle m \rangle$-H curve fitting on Windows platform is given in this section. The program language is Microsoft Visual Basic (Version 2.0J).

```
Global X0 As Integer
Global X1 As Integer
Global Y0 As Integer
Global Y1 As Integer
Global data_number As Integer
Global Wa As Double 'chi-square
Global Wa_min As Double 'least-chi-square
Global Degree_of_freedom As Integer
Global Reduced_chi_square As Double
Global Laser_Intensity(1000) As Single
Global Normalized_Intensity(1000) As Double
Global Magnetic_field_data(1000) As Double
Global Magnetic_steps(1000) As Integer
Global Sigma(1000) As Double
Global MaX_Field As Single
Global Normal_p As Single
Global Normal As Single
Global Normal_out As Single
Global Unit_X As Integer
Global Temperature As Double
Global Hs_init As Double
Global Hs As Double
Global NdX_p As Double
Global NdX As Double
Global NdX_init As Double
Global NdX_step As Double
Global NdX_max As Double
Global NdX_max_p As Double
Global NdX_min As Double
Global NdX_min_p As Double
Global NdX_out As Double
Global Order_Parameter As Double
Global Const K_b = 1.380658E-23
Global Input_File As String

Sub Calculation (Mag As Double, Delta_chi As Double, temp As Double)
```

```
Dim alpha As Double
Dim A As Double
Dim B As Double
Dim SI As Double
Dim T As Double
Dim dt As Double
Dim N As Double
Dim ex As Double
Dim ex1 As Double
Dim ex2 As Double

    alpha = (Delta_chi * Mag ^ 2) / (2 * K_b * temp)
    A = 0#
    B = 1#
    N = 2 ^ 12
    dt = (B - A) / N
    SI = 0#
    For j = 1 To N
T = A + dt * (j - 1) + dt / 2#
ex = Exp(alpha)
ex1 = ex ^ T
ex2 = ex1 ^ T       ' ex2 = Exp(alpha * t^2)
SI = SI + ex2 * dt
    Next
    Order_Parameter = (3# / (4# * alpha)) * (ex / SI - 1) - .5

End Sub

Sub Data_input ()
    Open Grain_main!FileIn.Text For Input As #1
i = 1
Do While Not EOF(1)
    Input #1, Magnetic_field_data(i), Laser_Intensity(i)
    i = i + 1
Loop
data_number = i - 1 ' データの数
    Close #1
    Normal_p = Laser_Intensity(i - 1)
    Grain_main!Normalization.Text = Format(Normal_p, "Scientific")
    Grain_main!MaxMag.Text = Magnetic_field_data(i - 1) * 10000#
    Normalize Normal_p ' 取り敢えず最後のデータでノーマライズする
End Sub

Sub Disp_Results ()
    FrmResult.Show
    Grain_main!Result_NdX.Text = Format(NdX_out, "Standard")
    Grain_main!Normal_now.Text = Format(Normal_out, "Scientific")
    Grain_main!Least.Text = Format(Wa_min, "Scientific")
    Grain_main!OutHs.Text = Format(Hs * 10000#, "Scientific")
    FrmResult!Text2.Text = Format(Temperature, "Standard")
    FrmResult!Text3.Text = Format(NdX_out * 1E-17, "Scientific")
    FrmResult!Text4.Text = Format(Hs * 10000#, "Scientific")
    FrmResult!Text5.Text = Format(Normal_out, "Scientific")
    FrmResult!Text6.Text = Format(Wa_min, "Scientific")
    FrmResult!Text7.Text = Format(Degree_of_freedom, "Scientific")
    FrmResult!Text1.Text = Format(Reduced_chi_square, "Scientific")
End Sub

Sub Fitting ()
```

```
Dim Norm As Single
Dim Norm_min As Single
Dim Norm_max As Single
Dim Norm_step As Single
Dim NdX_p As Double
Dim NdX_i As Integer
Dim NdX_min_i As Integer
Dim NdX_max_i As Integer
Dim NdX_step_i As Integer
Dim H As Double
Dim L As Integer
Dim IRO As Single
Dim R As Single
Dim Dummy As Integer

    Norm_min = Normal * .98
    Norm_max = Normal * 1.02
    Norm_step = Abs(Norm_max - Norm_min) / 4
    NdX_min_i = NdX_min * 1E+20     ' 1E+20をかけて整数部だけ取り出す
    NdX_max_i = NdX_max * 1E+20     ' 1000のオーダーの整数になっているはず
    NdX_step = Val(Grain_main!Calc_step)
    NdX_step_i = NdX_step * 1000    ' stepは100

    Wa_min = 1.7E+308               ' Doubleの最大値
    Grain_main!OutHs.Text = 0

    If Grain_main!Fix_chk.Value = 1 Then    'NormalizationをFIXする
Norm_min = Normal                   '
Norm_step = 3.4E+38                 'Singleの最大値
    End If

    For Norm = Norm_min To Norm_max Step Norm_step
Grain_main!Normal_now.Text = Format(Norm, "Scientific")
Normalize Norm  'Normalizationを変えてプロットしなおす
FrmPlot!Picture1.Cls
Plot_Preview

For NdX_i = NdX_min_i To NdX_max_i Step NdX_step_i
    Grain_main!Result_NdX.Text = Format(NdX_i * .001, "Standard")
    NdX_p = NdX_i * 1E-20   'NdX_pは1e-17オーダーの値
    Wa = 0#
    reference_mag = -999
    j = 0
    For i = 1 To data_number
H = Magnetic_field_data(i)
Calculation H, NdX_p, Temperature
If H <> reference_mag Then
    reference_mag = H
    j = j + 1
End If
Wa = Wa + ((Order_Parameter - Normalized_Intensity(i))^ 2)
 / Sigma(j)
L = 1           'Circleを描くとき1
IRO = &HFF&     '赤
R = 3           'Circleの半径
Plot H, Order_Parameter, L, IRO, R, Dummy
    Next
```

```
    If Wa <= Wa_min Then
Wa_min = Wa      'Least-chi-squareのこと
NdX_out = NdX_i * .001
Normal_out = Norm
If Grain_main!Fix_chk.Value = 1 Then
    parameter = 1
Else
    parameter = 2
End If
Degree_of_freedom = data_number - parameter
Reduced_chi_square = Wa_min / Degree_of_freedom
    End If
    Grain_main!Least.Text = Format(Wa_min, "Scientific")
    Grain_main!Not_least.Text = Format(Wa, "Scientific")
Next
    Next
    Hs = Sqr(15# * K_b * Temperature / (NdX_out * 1E-17))
    Grain_main!OutHs.Text = Format(Hs * 10000, "Scientific")
End Sub

Sub Hs_initial ()
    Sa_min = 9999999
    For i = 1 To data_number
Sa = Abs(Normalized_Intensity(i) - .8) ' <m>=0.8に一番近いデータを探す
If Sa <= Sa_min Then
    Sa_min = Sa
    I_min = i
End If
    Next

    ' <m>=0.8がどの測点の間にあるか調べる
    A = Normalized_Intensity(I_min + 1) - .8
    B = Sa_min
    C = Normalized_Intensity(I_min - 1) - .8

    If A * B < 0 Then
IP = I_min + 1
im = I_min
    End If
    If B * C < 0 Then
IP = I_min
im = I_min - 1
    End If

    ' フィッティングパラメータの大まかな値を計算しておこう
    Hs1 = Magnetic_field_data(IP)
    Hs0 = Magnetic_field_data(im)
    Hs_init = Hs0 + (Hs1 - Hs0) * (.8 - Normalized_Intensity(im)) /
    (Normalized_Intensity(IP) - Normalized_Intensity(im))
    NdX_init = 15 * K_b * Temperature / (Hs_init ^ 2)
    NdX_max_p = NdX_init * 1.1
    NdX_min_p = NdX_init * .9

    Grain_main!OutHs.Text = Format(Hs_init * 10000#, "Scientific")
    Grain_main!Result_NdX.Text = Format(NdX_init * 1E+17, "Standard")
    Grain_main!NdX0.Text = Format(NdX_min_p * 1E+17, "Standard")
    Grain_main!NdX1.Text = Format(NdX_max_p * 1E+17, "Standard")

End Sub
```

```
Sub Normalize (Norm As Single)

Dim reference As Double
Static Sum(1000) As Single
Static Mean(1000) As Single
Static Triger(50) As Integer
Static offset(50) As Integer

    reference = -999
    j = 0

    For j = 1 To data_number
' 取り敢えず、最終データで規格化
Normalized_Intensity(j) = Laser_Intensity(j) / Norm

' 入力データの統計
 If Magnetic_field_data(i) <> reference Then
    reference = Magnetic_field_data(i)
    k = k + 1
 End If
 Triger(k) = Triger(k) + 1
 Sum(k) = Sum(k) + Normalized_Intensity(j)
    Next j

    Magnetic_step = k

    ' 各磁場での測定値の母平均
    For j = 1 To Magnetic_step
Mean(j) = Sum(j) / Triger(j)
offset(j) = offset(j - 1) + Triger(j - 1) + 1
    Next j

    ' 各磁場での測定値の分散
    For j = 1 To Magnetic_step
        For k = offset(j) To offset(j) + Triger(j) - 1
    Sigma(j) = Sigma(j) + (Normalized_Intensity(k) - Mean(j)) ^ 2
        Next k
    Next j

End Sub

Sub Plot (X As Double, Y As Double, CL As Integer, Color As Single,
Radi As Single, k As Integer) ' ＧＸ，ＧＹに円を描く
Static GX
Static GY
Static GX0
Static GY0

    GX = X0 + (X1 - X0) / (MaX_Field / 10000) * X
    GY = Y1 - (Y1 - Y0) / 1.1 * Y

    Select Case CL
Case 1
    FrmPlot!Picture1.Circle (GX, GY), Radi, Color
Case 2
    FrmPlot!Picture1.PSet (GX, GY), Color
Case 3
    If k = 0 Then
```

```
FrmPlot!Picture1.PSet (X0, Y1), Color
    Else
FrmPlot!Picture1.Line -(GX, GY), Color
    End If
    End Select
End Sub

Sub Plot_Preview ()
Dim Plottype As Integer
Dim GX As Single
Dim GY As Single
Dim Color As Single
Dim Radius As Single
Dim Dummy As Integer

    X0 = 40: Y0 = 40: X1 = 600: Y1 = 340
    FrmPlot!Picture1.Line (X0, Y1)-(X1, Y1), &H0&
    FrmPlot!Picture1.Line (X0, Y0)-(X0, Y1), &H0&
    FrmPlot!Picture1.Line (X1, Y1)-(X1, Y0), &H0&
    FrmPlot!Picture1.Line (X0, Y0)-(X1, Y0), &H0&

    Unit_X = MaX_Field / 100            '   X軸は１００G毎に目盛 りを描 く
    If MaX_Field > 10000 Then
        Unit_X = MaX_Field / 1000       '   １T以上の時は１０００G毎
    End If

    For memorix = 0 To Unit_X Step 1
X = X0 + (X1 - X0) / Unit_X * memorix
If (memorix Mod 5) = 0 Then     '   50G毎の目盛 りは少し長 くします
    FrmPlot!Picture1.Line (X, Y1)-(X, Y1 - 8), &H0&
    FrmPlot!Picture1.Line (X, Y0)-(X, Y0 + 8), &H0&
    If (memorix Mod 10) = 0 Then
FrmPlot!Picture1.CurrentX = X - 25
FrmPlot!Picture1.CurrentY = Y1 + 5
FrmPlot!Picture1.Print MaX_Field * memorix / Unit_X ' X軸
    End If
End If
FrmPlot!Picture1.Line (X, Y1)-(X, Y1 - 5), &H0&
FrmPlot!Picture1.Line (X, Y0)-(X, Y0 + 5), &H0&
    Next

FrmPlot!Picture1.CurrentX = X1 - 40
FrmPlot!Picture1.CurrentY = Y1 + 30
FrmPlot!Picture1.Print "[ Gauss ]"

    For memoriy = 0 To 1.1 Step .1      '   Y軸は０．１毎に目盛 りを描 く
If memoriy = .6 Then            '   < m > = 0.5の目盛 りは少しだけ長 く
    FrmPlot!Picture1.Line (X0, Y)-(X0 + 8, Y), &H0&
    FrmPlot!Picture1.Line (X1, Y)-(X1 - 8, Y), &H0&
    FrmPlot!Picture1.CurrentX = X0 - 30
    FrmPlot!Picture1.CurrentY = Y - 10
    FrmPlot!Picture1.Print "0.5"
End If
Y = Y1 - (Y1 - Y0) / 1.1 * memoriy
FrmPlot!Picture1.Line (X0, Y)-(X0 + 5, Y), &H0&
FrmPlot!Picture1.Line (X1, Y)-(X1 - 5, Y), &H0&
    Next

    M1 = Y1 - (Y1 - Y0) / 1.1           '   < m > = 1 に線を引 く
```

```
    FrmPlot!Picture1.Line (X0, M1)-(X1, M1), &HFF&

    FrmPlot!Picture1.CurrentX = X0 - 30
    FrmPlot!Picture1.CurrentY = M1 - 10
    FrmPlot!Picture1.Print 1

    Plottype = 1              '測点のプロット
    Color = &HFF00&           ' みどり
    Radius = 5
    For j = 1 To data_number
Plot Magnetic_field_data(j), Normalized_Intensity(j),
Plottype, Color, Radius, Dummy
    Next
End Sub

Sub Results_Plot ()
Dim Plot_H As Double
Dim Plot_NdX As Double
Dim Hstep As Single
Dim H As Single
Dim CL As Integer
Dim Color As Single
Dim R As Single
Dim Dummy As Integer

    FrmPlot!Picture1.Cls

    Normalize Normal_out
    Plot_Preview

    Plot_NdX = NdX_out * 1E-17
    Hstep = MaX_Field / 50#
    Dummy = 0
    For H = .1 To MaX_Field Step Hstep
Plot_H = H / 10000#
Calculation Plot_H, Plot_NdX, Temperature
CL = 3            ' Lineを描くFlag
Color = &HFF&
Plot Plot_H, Order_Parameter, CL, Color, R, Dummy
Dummy = Dummy + 1
    Next

    Plot_Preview     ' Lineの上に円を重ね書きするため、もう一度Plotする

End Sub
```

Appendix B

Development of Experimental Setup in Low Temperature

The schematic representation of the developping experimental setup in lowtemperature is shown in Figure B.1. Four GP-IB instruments (two power supplies and two digital volt meters) are controlled with one controllar (Personal Computer; PC98). The system is devided with three parts colored different gradation in Figure B.1. First is the temperature control, second is the magnetic field contorol and third is the data acquiisition system. The main part of the of the computer program is the temperature control routine. The part of the source code is also given in following pages.

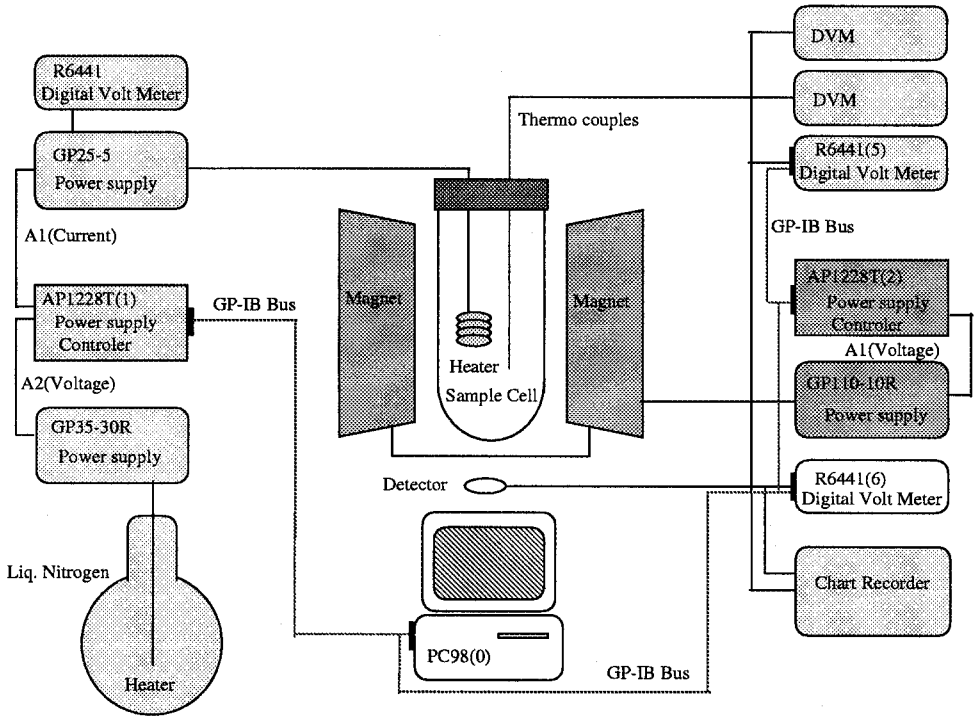

Figure B.1: Developping setup in low temperature.

```
70 CLS 3 : CONSOLE 0,25,1,1 : SCREEN 3 : COLOR ,,,1
80 KEY 1, "File": KEY 2 , "Start": KEY 3 , "Chage": KEY 4, "End"
90 KEY 5, "REF"  : KEY 6 , "HC"   : KEY 7 , "TEMP"
100 DIM TV(301),SMV(601),TMP(20)
110 OPEN "DUMMY1.DAT" AS #1
120 OPEN "TEMP.DAT" FOR OUTPUT AS #2 : PRINT #2 , TIME$
130 '******  磁場 vs 電圧の式 *****
140 DEF FNMAG2C(M)=M/.0365
150 DEF FNC2MAG(C)=C*.0365
160 CL=0
170 XSCALE = 9000                                ' Full scale of X-axis
180 YSCALE = 300                                 ' Full scale of Y-axis
190 YSCALED = .1                                 ' Full scale of YD-axis
191 YSCALER = .4
192 RT=.2
200 '************************************
210 '    Main
220 '************************************
230 GOSUB *GPIBINIT
240 GOSUB *TABLEREAD
250 GOSUB *LINEDRAW
260 GOSUB *SETTING
270 '冷却開始
280 NVR = 1 : HCR = 1
290 GOSUB *COOL
300 LOCATE 35,1 : PRINT "TGT=",TGT
310 KEY ON
320 ON KEY GOSUB 350,410,500,550      ' ファイル,測定,変更,終了,NV,HC,TEMP
330 GOTO 290
340 END
350 '**********************************
360 '  出力ファイル指定
370 '**********************************
380 GOSUB *FOPEN
390 CLS 1 ': LOCATE 0,1 : PRINT "Now Cooling "
400 RETURN
410 '**********************************
420 '  測定開始
430 '**********************************
440 CLS 1 ': LOCATE 0,1 : PRINT "測定中"
450 CNT = 0
460 PRINT #1,TIME$,"Start of measure"   'Start time
470 GOSUB *MEASURE
480 PRINT #1,TIME$,"End of measure"     'End time
490 RETURN
500 '**********************************
510 '  設定温度／磁場変更
520 '**********************************
530 GOSUB *SETTING
540 RETURN
550 '**********************************
560 '  プログラムの終了
570 '**********************************
580 PRINT @ADD1 ; "A1D0" , "A2D0"
590 PRINT @ADD2 ; "A1D0"
600 PRINT #2, TIME$ : CLOSE #1: CLOSE #2
610 END
620 '**********************************
630 '  ファイルオープン
640 '**********************************
```

```
650 *FOPEN
660 CLOSE #1
670 INPUT "File_Name(.DAT)"; OUTFNAME$
680 OPEN OUTFNAME$ + ".DAT" FOR OUTPUT AS #1
690 RETURN
700 '***********************************
710 '  ＧＰ－ＩＢ初期化
720 '***********************************
730 *GPIBINIT
740 ISET IFC
750 ISET REN
760 WBYTE &H14;
770 CMD DELIM=0
780 CMD TIMEOUT=20
790 ADD1 = 1 '温度制御用電源     A1:GP025-5 A2:GP035-30R
800 ADD2 = 2 'Magnet制御用電源   A1:GP110-10R
810 ADD5 = 5 '熱電対モニター用デジボル R6441A
820 ADD6 = 6 'Detector用デジボル       R6441A
830 PRINT @ADD5 ; "C"
840 PRINT @ADD6 ; "C"
850 PRINT @ADD5 ; "Z"
860 PRINT @ADD6 ; "Z"
870 PRINT @ADD1 ; "A1D0","A2D0"
880 PRINT @ADD2 ; "A1D0"
890 PRINT @ADD5 ; "F1,R0,M0,PR3,RE4"
900 PRINT @ADD6 ; "F1,R0,M0,PR3,RE4"
910 RETURN
920 '***********************************
930 '   TABLE読み込み
940 '***********************************
950 *TABLEREAD
960 FOR I=1 TO 300
970   READ TV(I)
980 NEXT I
990 RETURN
1000 '***********************************
1010 '  温度&測定条件設定
1020 '***********************************
1030 *SETTING
1040 GOSUB *TEMPSET
1050 GOSUB *MAGNETSET
1060 RETURN
1070 '***********************************
1080 '  温度設定
1090 '***********************************
1100 *TEMPSET
1110 LOCATE 0,1 : PRINT "設定温度"
1120 LOCATE 0,2 : PRINT "冷却電源電圧"
1130 LOCATE 0,3 : PRINT "CELL内ヒーター電流"
1131 LOCATE 0,4 : PRINT "alpha"
1132 LOCATE 0,5 : PRINT "refer"
1140 LOCATE 0,10: INPUT "Hit return key" ; A$
1150 IF A$ ="" THEN GOTO 1160
1160 LOCATE 0,1 : INPUT "設定温度"          ; TGT   'TarGet Temperature
1170 LOCATE 0,2 : INPUT "冷却電源電圧"      ; NV    'N2 Voltage
1180 LOCATE 0,3 : INPUT "CELL内ヒーター電流"; HC    'Heater Current
1190 LOCATE 0,4 : INPUT "alpha"; ALPHA
1195 LOCATE 0,5 : INPUT "refer"; RT
1200 LOCATE 0,10 : INPUT "これでいい ?(Y/N)"; YNA$
```

```
1210 IF YNA$ ="N" THEN CLS 1 : GOTO 1110
1220 NV0 = NV : HC0 = HC                          ' Initial value of NV & HC
1230 INTEMP=TGT
1240 GOSUB *TEMP2VOLT
1250 SV=OUTVOLT
1260 NVSTP = INT(NV * 2000 / 35)
1270 HCSTP = INT(HC * 2000 / 5)
1280 LOCATE 0,7 : PRINT "Target Voltage of Thermo-couple ",SV*1000,"mV"
1290 LOCATE 0,9 : INPUT "Hit return key!" ; A$
1300 IF A$ = "" THEN CLS 1
1310 LINE(X0,Y0-(Y0-Y1)/YSCALE*(TGT-T0))-(X1,Y0-(Y0-Y1)/YSCALE*(TGT-T0)),2
1320 RETURN
1330 '***********************************
1340 '   MAGNET 設定
1350 '***********************************
1360 *MAGNETSET
1370 LOCATE 0,1 : PRINT "磁場"
1380 LOCATE 0,2 : PRINT "磁場上昇のステップ"
1390 LOCATE 0,3 : PRINT "Triger 回数"
1400 LOCATE 0,5 : INPUT "Hit Return Key" ; B$
1410 IF B$ = "" THEN GOTO 1420
1420 LOCATE 0,1 : INPUT "磁場"; MMAX
1430 LOCATE 0,2 : INPUT "磁場上昇のステップ";STP
1440 LOCATE 0,3 : INPUT "Triger 回数"; TRG
1450 LOCATE 0,5 : INPUT "これでいい ?(Y/N)" ; YNB$
1460 IF YNB$ = "N" THEN CLS 1 : GOTO 1370
1470 INMAG=MMAX
1480 GOSUB *MAG2CUR
1490 MAGC = OUTCURM
1500 LOCATE 0,7 : PRINT "磁石の電流は",MAGC,"Ampere まで上が ります"
1510 LOCATE 0,9 : INPUT "Hit return key" ; B$
1520 IF B$ = "" THEN CLS 1
1530 RETURN
1540 '***********************************
1550 '   冷却
1560 '***********************************
1570 *COOL
1580 GOSUB *N2HEATUP
1590 GOSUB *TRIGER5
1600 REF = TEMP - TGT
1610 DTDT = (TEMP-MEANT)/10
1620 'gosub *saturation
1630 IF REF => 0 THEN GOSUB *REFPLUS
1640 IF REF <  0 THEN GOSUB *REFMINUS
1650 'IF ABS(Temp-TGT)<=.1 THEN BEEP
1660 GOSUB *CELLHEATUP
1670 RETURN
1680 '***********************************
1690 '   測定の本体
1700 '***********************************
1710 *MEASURE
1711 FOR IM1=0 TO 50
1712     GOSUB *TRIGER6
1713     GOSUB *COOL
1714     CNT=CNT+1
1715     'FOR DUMMY=0 TO 1000 : NEXT DUMMY
1716 NEXT IM1
1720 FOR UP=0 TO 2000 STEP 2000/STP
1730   GOSUB *MAGFIELDUP
```

```
1740   FOR DUMMY = 0 TO 1000 : NEXT DUMMY
1750   FOR MI= 1 TO TRG
1760     GOSUB *TRIGER6
1770     GOSUB *COOL
1780     CNT = CNT + 1
1790     FOR DUMMY=0 TO 1000 : NEXT DUMMY
1800   NEXT MI
1810 NEXT UP
1820 GOSUB *MAGFIELDDOWN
1821 FOR IM2=0 TO 200
1822    GOSUB *TRIGER6
1823    GOSUB *COOL
1824    CNT=CNT+1
1825   ' FOR DUMMY=0 TO 1000 : NEXT DUMMY
1826 NEXT IM2
1830 RETURN
1840 '************************************
1850 *REFPLUS
1860 '************************************
1870 NV = NV0 : FLAG = 1
1880 GOSUB *NVCTRL
1890 HC=0
1910 GOSUB *HCCTRL
1920 RETURN
1930 '************************************
1940 *REFMINUS
1950 '************************************
1960 'HC = HC0
1970 FLAG = -1
1980 IF DTDT<0 THEN HC=ABS(REF)*ALPHA
1990 IF DTDT>0 THEN HC=0
2000 GOSUB *HCCTRL
2010 GOSUB *NVCTRL
2020 RETURN
2030 '************************************
2040 '  窒素内ヒーター上昇
2050 '************************************
2060 *N2HEATUP
2070 NVSTP = INT(NV * 2000 / 35)
2080 VV$ = STR$(NVSTP)    'VV : Voltage of Vessel
2090 PRINT @ADD1 ; "A2D"+VV$
2100 RETURN
2110 '************************************
2120 '  Ｃｅｌｌ内ヒーター制御
2130 '************************************
2140 *CELLHEATUP
2150 HCSTP = INT(HC * 2000 / 5 )
2160 CC$ = STR$(HCSTP)                    'CC : Current of Cell-heater
2170 PRINT @ADD1 ; "A1D"+CC$
2180 RETURN
2190 '********************************************
2200 ' Control of voltage of vessel :5%UP
2210 '********************************************
2220 *NVCTRL
2230 IF NV > 10 THEN NV=10 : GOTO 2240  'Software Fuse
2240 RETURN
2250 '********************************************
2260 ' Control of current of Cell heater 5% up&down
2270 '********************************************
2280 *HCCTRL
```

```
2290 IF HC > 3 THEN HC=3 : GOTO 2300 ' Software Fuse
2300 RETURN
2310 '**********************************
2320 '  時間変化が平衡に達したか？
2330 '**********************************
2340 *SATURATION
2350 RETURN
2360 '**********************************
2370 ' Saturation clear
2380 '**********************************
2390 *SMVCLS
2400 'FOR ISMV=1 TO 499
2410 '  SMV(ISMV)=0
2420 'NEXT ISMV
2430 'SAT = 0
2440 RETURN
2450 '**********************************
2460 '  温度→電圧 : INTEMP -> OUTVOLT
2470 '**********************************
2480 *TEMP2VOLT
2490 TR = INT(INTEMP)
2500 TR1=TR+1
2510 MUVOLT = TV(TR)+(TV(TR+1)-TV(TR)) * (INTEMP-TR)   ' μ V
2520 OUTVOLT = MUVOLT * .000001                         ' μ V -> V
2530 RETURN
2540 '**********************************
2550 '  電圧→温度 : INVOLT -> OUTTEMP
2560 '**********************************
2570 *VOLT2TEMP
2580 V = INVOLT * 1E+06              'V -> μ V
2590 FOR I=1 TO 300
2600   SA = V - TV(I)
2610   IF SA < 0 THEN TI=I-1 : GOTO 2630
2620 NEXT I
2630 OUTTEMP = TI + ( V - TV(TI) ) / ( TV(TI+1) - TV(TI) )
2640 RETURN
2650 '**********************************
2660 '  磁場上昇
2670 '**********************************
2680 *MAGFIELDUP
2690 MUP$=STR$(UP)
2700 PRINT @ADD2 ; "A1D"+MUP$
2710 INCURM = UP / 2000 * 10!
2720 GOSUB *CUR2MAG
2730 RETURN
2740 '**********************************
2750 '  磁場降下
2760 '**********************************
2770 *MAGFIELDDOWN
2780 FOR I=2000 TO 0 STEP -100
2790   FOR DUMMY=0 TO 1000 : NEXT DUMMY
2800   MDOWN$=STR$(I)
2810   PRINT @ADD2 ; "A1D"+MDOWN$
2820 NEXT I
2830 CLS 1 : LOCATE 0,1 : PRINT "測定終了"
2840 RETURN
2850 '**********************************
2860 '  Triger5 : 熱電対モニター
2870 '**********************************
2880 *TRIGER5
```

```
2890 PRINT @ADD5 ; "E"
2900 INPUT @ADD5 ; THVOLTC$
2910 TH$=MID$(THVOLTC$,4,14)
2920 THVOLT=VAL(TH$)
2930 INVOLT=THVOLT
2940 GOSUB *VOLT2TEMP
2950 TEMP=OUTTEMP
2960 PRINT #2,CNT0,TEMP,THVOLT,DTDT
2970 LOCATE 35,19 : PRINT USING "@=#####";"No.",CNT0
2975 LOCATE 50,19 : PRINT USING "@=####.###";"TEMP",TEMP
2980 LOCATE 35,21 : PRINT USING "@=#####";"NV",NV
2985 LOCATE 50,21 : PRINT USING "@=##.####";"HC",HC
2990 LOCATE 50,20 : PRINT USING "@=##.#####^^^^";"dT/dt",DTDT
2995 LOCATE 35,20 : PRINT USING "@=####.###";"REF",REF
2996 LOCATE 35,22 : PRINT USING "@=#.##";"alpha",ALPHA
3000 'LOCATE 35,22 : PRINT "CTM",CTMINUS
3010 CNT0 = CNT0 + 1
3020 GOSUB *PLOT
3030 GOSUB *PLOTD
3040 SUMT=0
3050 FOR I=1 TO 19
3060   TMP(I)=TMP(I+1)
3070   SUMT=SUMT+TMP(I)
3080 NEXT I
3090 TMP(20)=TEMP
3100 SUMT=SUMT+TMP(20)
3110 MEANT=SUMT/20
3120 RETURN
3130 '*********************************
3140 '   Triger6  : Monitor of PhotoDiode
3150 '*********************************
3160 *TRIGER6
3170   PRINT @ADD6 ; "E"
3180   INPUT @ADD6 ; PDVOLTC$
3190   PD$=MID$(PDVOLTC$,4,14)
3200   PDVOLT=VAL(PD$)
3210   PRINT #1, OUTMAG,PDVOLT,TEMP,CNT
3220 RETURN
3230 '*********************************
3240 '   DUMMY LOOP
3250 '*********************************
3260 *DUMMY
3270 FOR DUMMY=0 TO 100000! : NEXT DUMMY
3280 RETURN
3290 '*********************************
3300 '   磁場→電流
3310 '*********************************
3320 *MAG2CUR
3330 OUTCURM=FNMAG2C(INMAG)
3340 RETURN
3350 '*********************************
3360 '   電流→磁場
3370 '*********************************
3380 *CUR2MAG
3390 OUTMAG=FNC2MAG(INCURM)
3400 RETURN
3410 '*********************************
```